Sniff-invariant intensity perception using olfactory bulb coding of inhalation dynamics

Rebecca Jordan[1,2], Mihaly Kollo[1,2] and Andreas T Schaefer[1,2]

1. Neurophysiology of Behaviour Laboratory, Francis Crick Institute, London, UK
2. Department of Neuroscience, Physiology & Pharmacology, University College London, UK

Correspondence and requests for materials, including custom software, should be addressed to A.T.S via email to andreas.schaefer@crick.ac.uk.

Summary

For stable perception of odor intensity, there must exist a neural correlate that is invariant across other parameters, such as the highly variable sniff cycle. Previous hypotheses suggest that variance in inhalation dynamics alters odor concentration profiles in the naris despite a constant environmental concentration. Using whole cell recordings in the olfactory bulb of awake mice, we directly demonstrate that increased sniffing frequency mimics the effect of odor concentration increase at the level of both mitral and tufted cell (MTC) firing rate responses and temporal responses. In contrast, we find that mice are capable of discriminating concentrations within short timescales despite highly variable sniffing behavior. We reason that the only way mice can differentiate a change in sniff parameters and a change in concentration is to encode information about the inhalation parameters in parallel. While conceivably this could be achieved via corollary discharge from respiration control centres, we find that the sniff-driven activity of MTCs without odor input is informative of the kind of inhalation that just occurred, allowing rapid detection of a change in inhalation. Thus, a possible reason for sniff modulation of the early olfactory system may be to inform downstream centres of nasal flow dynamics, so that an inference can be made about environmental concentration independent of sniff variance.

Introduction

For consistency of perception, sensory systems must be able to stably encode the same perceptual features across a wide range of situations. An example of this is the encoding of object size independent of object distance in the visual system (Helmholtz, 1867) – we do not perceive a giant apple when viewed at close range, and similarly we do not misperceive buildings as tiny objects when viewed from great distance. In the olfactory system, studies have looked at how odor identity may be encoded independent of odor concentration (Cleland et al., 2012; Uchida and Mainen, 2008; Wachowiak et al., 2002; Wilson et al., 2017) and sniff cycle variance (Cury and Uchida, 2010). An olfactory problem that has received less attention, however, is stable encoding of odor intensity – the perceptual correlate of odor concentration (Wojcik and Sirotin, 2014). Increasing concentration is known to affect neural activity in many ways (Mainland et al., 2014). At the level of glomerular input from olfactory sensory neurons (OSNs), increasing concentration enhances the activity of already responsive glomeruli and incorporates new glomeruli into the activity profile, overall resulting in a broadening of the spatial 'map' of activity (Rubin and Katz, 1999; Spors and Grinvald, 2002). Changes in spike rate are also seen at the level of the olfactory bulb output cells, mitral and tufted cells (MTCs), though this can be a more complex mixture of inhibitory and excitatory effects (Bathellier et al., 2008; Cury and Uchida, 2010; Fukunaga et al., 2012; Meredith, 1986), and is thought to be constrained via inhibitory circuits (Kato et al., 2013; Miyamichi et al., 2013; Roland et al., 2016). The perhaps more ubiquitous correlates of concentration increase, however, are temporal response changes, notably with early excitation undergoing a latency reduction in OSNs (Ghatpande and Reisert, 2011; Rospars et al., 2000), MTCs (Cang and Isaacson, 2003; Fukunaga et al., 2012; Sirotin et al., 2015), as well as in the piriform cortex (Bolding and Franks, 2017). This is thought to arise since OSNs will depolarise to threshold more quickly when the concentration profile in the naris is steeper.

In awake mice, sniffing behaviour is in continual flux (Kepecs et al., 2007; Welker, 1964; Wesson et al., 2008a, 2009; Youngentob et al., 1987). This might present a problem for concentration coding: firstly,

50 changing flow will affect the number of odor molecules entering the nasal passage, altering the
51 concentration profile in the naris despite a stable environmental concentration (Mainland and Sobel,
52 2006; Shusterman et al., 2017; Teghtsoonian et al., 1978). Secondly, altering the velocity of air in the
53 naris will alter the time at which odorised air reaches the olfactory epithelium, which may disrupt the
54 reliability of temporal coding of concentration (Shusterman et al., 2017). Despite this, previous work
55 suggests that humans can perceive odor intensity independent of the inhalation flow rate
56 (Teghtsoonian et al., 1978). Here, using whole cell patch recordings in awake mice, we show that faster
57 sniffs evoke response changes identical to those caused by increasing concentration. Surprisingly
58 however, we show that variance in sniffing has little effect on the performance of mice trained to
59 make fine concentration discriminations. Finally, we propose that the olfactory system can make an
60 inference about whether a response change was caused by concentration change or sniff change by
61 encoding the parameters of sniffing on fast timescales in mitral and tufted cells, which respond to
62 inhalation change in cell-type specific ways, allowing rapid detection of a change in sniffing.

63 Results

64 *Changes in sniffing can mimic the effect of increased concentration on firing rate response*

65 We first wanted to determine whether the effect of sniff changes on MTC odor response could
66 qualitatively mimic concentration changes at the level of FR change. To do this, we used whole cell
67 recordings from identified MTCs in awake passive mice, as this allows unbiased sampling from the
68 MTC population in terms of baseline firing rate (FR), and reliable identification of cell type based on
69 electrophysiology (Kollo et al., 2014; Margrie et al., 2002). On each trial, mice were presented
70 randomly with 2 s long odor stimuli calibrated to either 1% (low concentration) or 2.5% (high
71 concentration) square pulses. On a small percentage of low concentration trials, mice also received a
72 gentle air puff to the flank, evoking fast sniffing behavior characterised by high frequency sniffs and
73 short inhalation duration (Figure 1A and S1). For all analyses in the manuscript, 'odor onset' (t=0) is
74 defined as the first inhalation onset during the odor stimulus. Note that several parameters of sniffing

75 co-vary with inhalation duration, including the sniff duration, the previous sniff duration and the slope
76 of the inhalation (Figure S2). Thus wherever we refer to 'fast' or 'slow' sniffing, this will necessarily
77 refer to variance in these multiple parameters.

78 During recordings, it was apparent that some cells displayed overt changes in FR with the increase in
79 concentration, and the most salient of these were increases in excitatory FR response (Figure 1B, cell
80 a and cell b). When comparing changes in FR evoked by concentration increase to those taking place
81 as a result of increased sniff frequency, it was apparent that very similar changes took place (Figure
82 1B). Altogether we recorded from 20 MTC pairs in such a manner, with a range of FR responses to the
83 low concentration odorant (Figure 1C). Comparing heat maps of the changes in FR due to increased
84 concentration and due to increased sniff frequency revealed a very similar set of changes across the
85 dataset (Figure 1D), which were significantly correlated compared to shuffle controls ($R = 0.63$, $p =$
86 $5x10^{-19}$; Figure 1E; see methods). When taking a broad measure of the change in firing rate across the
87 first second of the stimulus, changes in FR were significantly correlated between those resulting from
88 concentration increase and those resulting from faster sniffing ($R^2 = 0.62$, $p = 5x10^{-5}$, $n = 20$; Figure 1F).

89 While in the output of MTCs the effect of sniffing and concentration increase were very similar,
90 differences were seen in the subthreshold response changes, suggesting that changes in input in the
91 two cases were not identical: increases in inhibition were generally larger for concentration increase
92 than for faster sniffing (Figure S3). We suggest this could be the result of inhibitory networks which
93 act to normalise olfactory bulb output (within limits) in the face of increased input (Kato et al., 2013;
94 Miyamichi et al., 2013; Roland et al., 2016).

95 Thus, while increased concentration causes greater increases in subthreshold inhibition than
96 increased sniff frequency, the latter results in changes in the olfactory bulb output that apparently
97 mimic those resulting from increases in concentration.

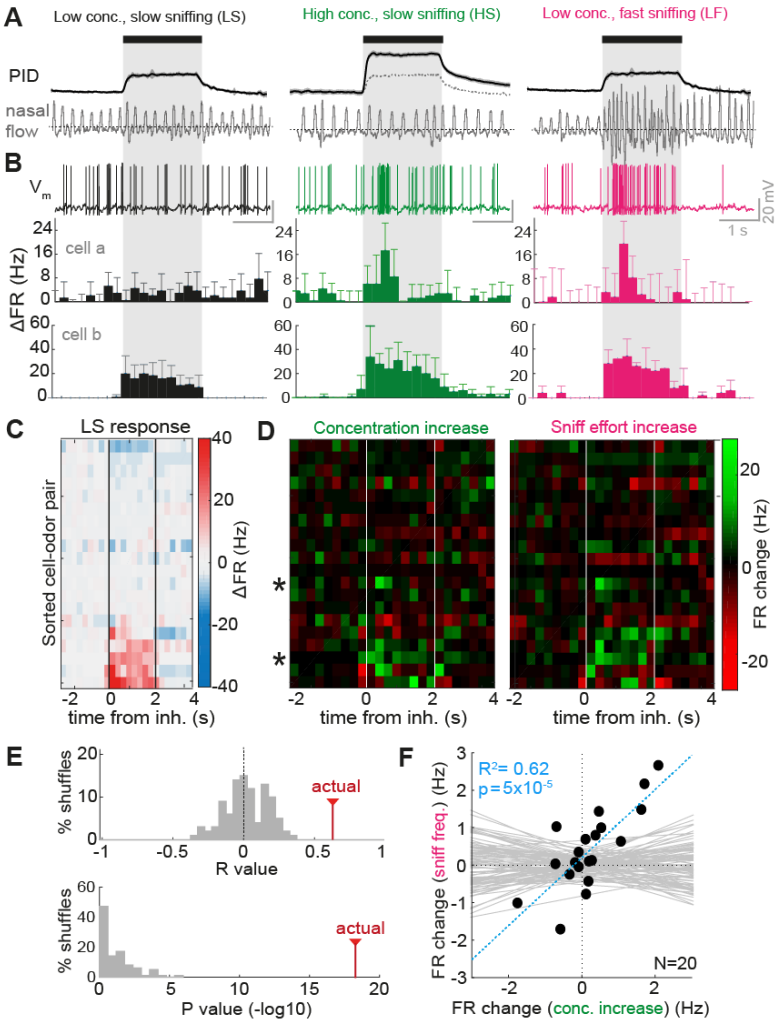

Figure 1. Sniff change and concentration change have similar effects on FR responses of MTCs

(**A**) Stimulation paradigm during whole cell recordings. PID traces show response of photoionisation detector (magnitude proportional to odor concentration), while nasal flow traces show example sniffing recorded using external flow sensor for the three types of trial. Black bar and grey box shows where odor is on, aligned to first inhalation onset. (**B**) Example odor responses recorded in each stimulus condition. V_m traces show example responses for cell a, while PSTHs below show averaged FR responses in 250 ms time bins for 5 trials in each case. Bottom-most PSTHs are calculated for a different example, cell b. Error bars show standard deviation. All are aligned to first inhalation onset. (**C**) Heatmap of average FR respones for all cell odor pairs in the low concentration slow sniff frequency condition (LS), ordered by mean FR response. (**D**) Heatmap of response changes (difference between PSTHs): Concentration increase = HS-LS, sniff frequency increase = LF-LS. Asterisks indicate cell a and cell b examples. (**E**) Top: R values for correlation across all odor time bins as shown in D, between FR change due to concentration change and those due to sniff frequency change. Histogram shows R values for shuffle controls, 'actual' shows R value for real data. Bottom: as for above, but histogram showing p-values for the correlations ($-\log_{10}$) (**F**) Correlation between mean FR response change for concentration change (HS-LS) and sniff frequency change (LF-LS) across first second of odor stimulus. N = 20 cell-odor pairs. Grey lines show correlations calculated for 100 shuffle controls, blue line shows real correlation.

98 ***Faster inhalation causes temporal shifts similar to those reported for concentration***

99 ***increase***

100 It has been reported that increased concentration causes changes in response on finer temporal
101 timescales, in particular the advance of excitatory bursts (Cang and Isaacson, 2003; Fukunaga et al.,
102 2012; Sirotin et al., 2015). Does a faster sniff similarly cause such temporal shifts on early timescales?

103 To determine this, we first analysed 13 cell-odor pairs with early excitatory responses recorded in
104 passive mice where only a single concentration stimulus (1% saturated vapour pressure) was
105 presented to the animal across trials. Comparing the FR response over the first 250 ms for 'fast' sniff
106 trials (>70th percentile peak inhalation slopes), and 'slow' sniff trials (<30th percentile), it was apparent
107 that faster inhalation could cause a latency advance of the excitatory burst (Figure 2A-B). Across all
108 cell-odor pairs, faster inhalation caused a significant latency reduction in mean response onset
109 (latency change (fast-slow) = -16 ± 14 ms, $p = 0.002$ paired t-test between onsets for slow and fast
110 inhalations; Figure 2C). Onset latencies displayed a significant relationship with the peak firing rate
111 during the response ($R^2 = 0.61$, $p = 0.002$, $n = 13$; Figure 2E), suggesting that the most strongly activated
112 cells respond earlier. The extent of the latency reduction for fast sniffing was significantly correlated
113 with the onset time during slow inhalation: if the response was of longer latency during slow sniffing,
114 the latency reduction was greater ($R^2 = 0.46$, $p = 0.01$, $n = 13$; Figure 2D). This indicates that those cell-
115 odor pairs showing a stable latency are likely already responding at the earliest timescale – i.e. there
116 is a lower limit on the latency of odor response.

117 It was previously shown in anaesthetized mice that mitral cells (MCs) undergo robust reductions in
118 latency of excitation for concentration increase, while tufted cells (TCs) – which already respond
119 earlier - do not (Fukunaga et al., 2012). We used sniff cycle phase preference boundaries to determine
120 putative MC (pMC) and TC (pTC) phenotype using subthreshold activity as previously described
121 (Fukunaga et al., 2012; Jordan et al., 2017). Examples could be found where both pMCs and pTCs
122 underwent reductions in latency of excitation when the sniff was fast (Figure 2A), however in general,

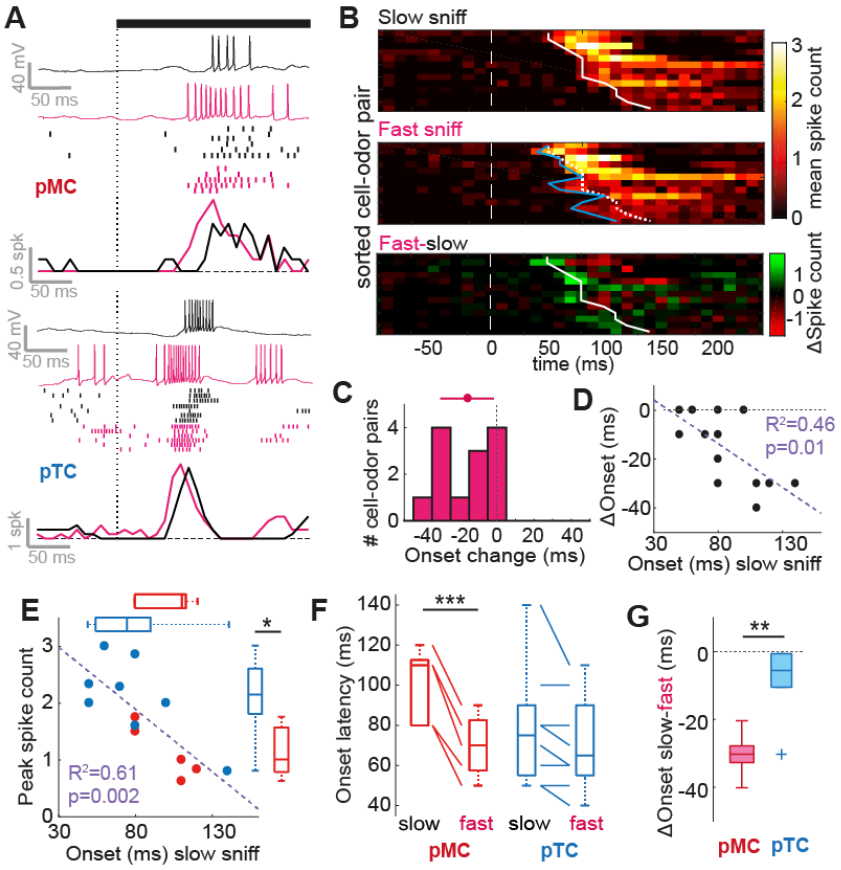

Figure 2. Faster inhalation causes temporal shifts similar to those reported for concentration increase

(**A**) Example V_m traces, spike rasters and mean spike counts for early excitatory responses for slow inhalation (black) and fast inhalation (pink), for two different cell-odor pairs. The top example is from a putative mitral cell (pMC) and bottom example is from a putative tufted cell (pTC). Rasters are ordered (top to bottom) by slowest to fastest inhalation. Black bar and dotted line indicate odor onset aligned to the first inhalation onset. (**B**) Heatmaps of mean spike count for 13 cell-odor pairs showing early excitation in response to slow inhalation (top) and fast inhalation (middle). White dashed line indicates odor onset aligned to the first inhalation onset. Cell odor pairs are sorted from short to long onset latency (during slow inhalation). Bottom heatmap shows the difference between the two above (fast-slow). White solid and dotted line indicates onset latency of each cell-odor pair for slow inhalation. Blue line indicates onset latency for fast inhalation. (**C**) Histogram of onset latency changes (fast-slow) for all 13 cell-odor pairs. (**D**) Scatter plot to show relationship between onset latency for slow inhalation, and the onset change between fast and slow inhalation. (**E**) Correlation between response onset latency and peak spike count for early excitatory odor responses evoked by a slow sniff. Blue data comes from pTCs and red data comes from pMCs. Boxplots compare the two parameters for pTCs and pMCs. (**F**) Comparison of response onset latencies for excitatory responses evoked by fast and slow sniffs for pMCs and pTCs. (**G**) Comparison of response onset latency change (fast-slow sniff) for pMCs and pTCs.

124 reductions for pMCs were greater than reductions for pTCs (pMCs: latency change = -30 ± 7 ms, p =
125 $7x10^{-4}$, paired t-test, n = 5 cell-odor pairs; pTCs: latency change = -8±10 ms, p = 0.08, paired t-test, n =
126 8 cell odor pairs; pMCs vs pTCs: p = 0.001, unpaired t-test; Figure 2F-G), and this was largely because
127 pTCs already tended to respond with shorter latency during slow sniffs than pMCs (pTC onset median
128 = 75 ms, IQR = 55-90 ms; pMC onset median = 110 ms, IQR = 80-113 ms, p = 0.13, Ranksum; Figure
129 2E).

130 Thus, the temporal shifts and cell-type specificity in the effect of faster sniffing matches that previously
131 described for concentration increases in anaesthetized mice (Fukunaga et al., 2012).

132 ***Faster inhalation mimics effect of concentration increase on latency response in the***
133 ***timescale of a single sniff***

134 Could the effect of sniffing on latency directly mimic concentration effects at this timescale? When
135 comparing high and low concentration stimuli over the first 250 ms in MTC recordings from passive
136 mice (dataset as in Figure 1), the only salient changes in response to increased concentration were
137 latency advances of excitatory burst stimuli (Figure 3A and B). When correlating changes in spike count
138 as before (Figure 1E) between those occurring for sniff change and those occurring for concentration
139 change, there was a highly significant positive correlation between the two (R = 0.71, p = $4x10^{-72}$, n =
140 525 time bins; Figure 3C). Latency reductions for concentration increase were similar in magnitude to
141 those seen due to sniff change (Figure 3D, mean onset advance = -18±10ms, p = 0.04, n = 4 paired t-
142 test between onsets for low and high concentration), and similar to those previously reported (Sirotin
143 et al., 2015). This latency change contributed to the entirety of the discriminability of the two different
144 concentrations on this timescale, with the Euclidean distance between the two dropping to baseline
145 if the excitatory bursts were manually shifted forward for the low concentration (Figure 3E, 'slow sniff'
146 vs 'slow sniff adv.', see methods). Faster inhalations during low concentration trials mimicked the
147 latency shifts caused by concentration increase, rendering the high and low concentration stimuli
148 indistinguishable (Figure 3E, 'slow sniff' vs 'fast sniff). Registering spikes to sniff cycle phase revealed

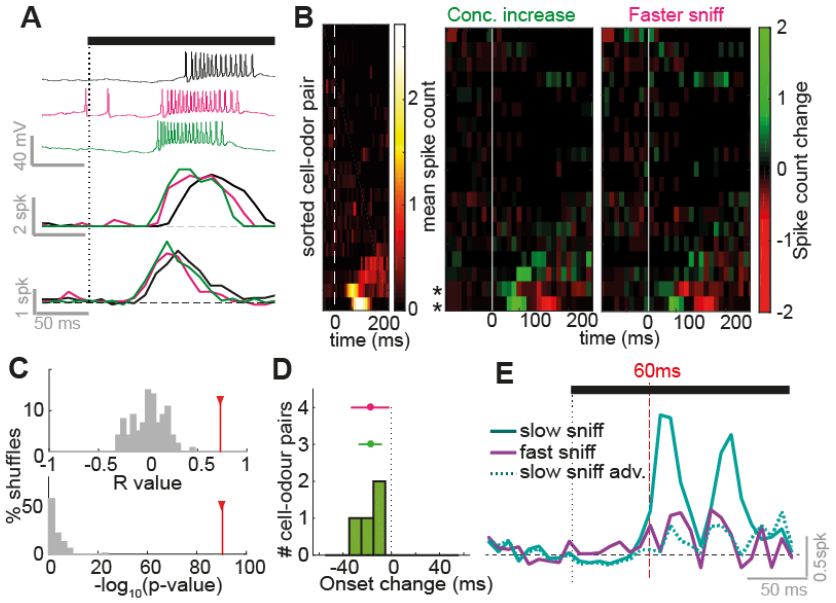

Figure 3. Inhalation change and concentration change cause similar temporal effects on early responses. (**A**) Example traces and mean spike counts for early excitatory responses. Black shows response at low concentration and slow inhalation, pink shows response at low concentration and fast inhalation, and green shows response for high concentration and slow inhalation. (**B**) Left: Heatmap to show early spike counts of all 20 cell-odor pairs recorded for low concentration and slow inhalation. Cell-odor pairs are sorted by the mean spike count during odor, from low to high. Middle: Heatmap to show difference in spike counts between high concentration and low concentration (slow inhalation). Left: heatmap to show difference in spike count between fast inhalation and slow inhalation (low concentration). (**C**) Top: R values for correlation across all odor time bins as shown in B, between spike count change due to concentration increase and due to faster inhalation. Histogram shows R values for shuffle controls, red bars show R value for real data. Bottom: as for above, but histogram showing p-values for the correlations ($-\log_{10}$). (**D**) Histogram to show response onset changes due to concentration increase. Errorbar in green shows mean and SD of this data, and in pink shows the distribution of changes as in panel C for comparison. (**E**) Euclidean distance between population spike count response vectors for high and low concentration (slow inhalation; 'slow sniff', solid cyan), for high concentration and time-shifted low concentration ('slow sniff adv.'; where excitatory latency changes due to concentration change were undone via time shifting of the data; dotted cyan), and for high concentration and low concentration where low concentration data came from fast inhalation trials ('fast sniff'; solid purple).

a potential increase in the ability to detect changes in concentration despite changes in sniffing (Figure S4; supplementary information), suggesting that the OB may require information about sniff

152 parameters in order to determine the concentration. Thus, even on short timescales, a more rapid
153 inhalation mimics concentration increases at the level of the olfactory bulb output.

154 ***Mice can successfully discriminate concentrations on rapid timescales***

155 Rodents have previously demonstrated the ability to discriminate odor concentrations (Abraham et
156 al., 2004; Parthasarathy and Bhalla, 2013; Slotnick and Ptak, 1977; Wojcik and Sirotin, 2014). Given
157 the physiology (Figure 1-3), and that sniff parameters are constantly varying in awake mice
158 (Wachowiak, 2011), we next sought to determine the capabilities of mice to distinguish odor
159 concentrations in a simple go/no-go paradigm (Figure 4A-C), despite variance in sniffing.

160 First, mice were trained to simply distinguish high (3%) versus low (1%) concentration stimuli. 3 mice
161 were trained with the low concentration stimulus as the CS+ ('Low go'), and 5 mice were trained with
162 high concentration as the CS+ ('High go'). After pre-training (Figure S5A), all mice learned the
163 distinction within a single training session (Figure 4D; 85 ± 19 trials to 80% correct, n = 8). Mice also
164 made rapid decisions based on concentration: analysis of the reaction time of mice based on lick
165 probability showed that mice could perform the task successfully within as low as 200 ms (Figure 4E,
166 median = 300 ms, range = 200 to 1050 ms, see methods). Similarly, using divergence of sniffing
167 behavior between CS+ and CS- stimuli (see methods), reaction times could be estimated at 214 ± 60
168 ms, and as low as 160 ms (Figure 4F) - in every case the first exhalation already showing a significant
169 difference between CS+ and CS- stimuli. Thus mice can make decisions about concentration on the
170 timescale of a single inhalation.

171 Mice were not using flow changes from the olfactometer output to make the discrimination, as our
172 olfactometer design keeps flow from odor outlet constant (Figure 4G). Secondly, trigeminal
173 stimulation was likely not being used since mice subsequently learned to discriminate the same
174 concentrations of vanillin (an odor which is thought not to stimulate trigeminal afferents – Frasnelli et
175 al., 2011), within a significantly shorter timeframe (16 ± 14 trials to criterion, p = 0.001, paired t-test,
176 n = 6 mice, Figure 4H), suggesting they may generalise the 'task rule' for concentrations across

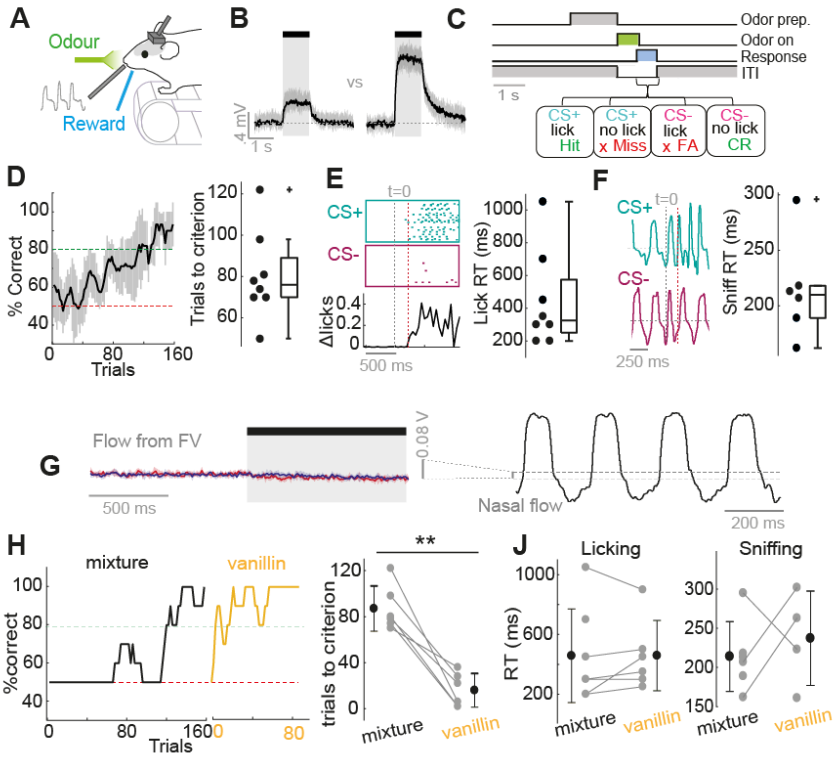

Figure 4. Mice rapidly learn to discriminate concentrations on fast timescales.

(**A**) Diagram of head-fixed behaviour (**B**) Average PID traces for concentration go/no-go stimuli. Shaded area shows standard deviation. (**C**) Concentration go/no-go task sequence. (**D**) Left: average learning curve for 8 mice. Percentage correct is calculated as a moving average over 5 CS+ and 5 CS- trials. Shaded area indicates SD. Right: distribution of learning times to criterion (4 successive learning curve points at or above 80% correct). (**E**) Left: example to show calculation of reaction time from lick behaviour. Rasters of licking during criterion performance are shown for CS+ and CS-. A difference in mean lick count over time is then calculated (bottom) and lick reaction time (RT) is determined where this difference first exceeds 2 SDs of the baseline difference. Red dotted line indicates RT calculated for this mouse. Right: distribution of lick RTs calculated in this way. (**F**) Left: example sniff traces for CS+ and CS- during driterion performance. Prior to licking mice show rapid sniff bouts such that RT may be determined earlier using divergence of sniff waveforms (see methods). Red dotted line indicates RT calculated for this mouse. Right: distribution of RTs calculated using sniff time divergence. (**G**) Mean flow change recorded 1 mm from olfactometer output for high concentration stimulus (red) and low concentration stimulus (blue). Average of 10 trials; shaded area shows standard deviation. Y scale bar is compared to that of nasal flow traces recorded in the same manner to demonstrate the negligible nature of flow change from the olfactometer. (**H**) Learning curves for an example mouse for 2-concentration discrimination, first for the odor mixture (in black) and subsequently for vanillin (yellow). Right hand plot compares the number of trials to criterion for the initial mixture and vanillin for each mouse. (**J**) Plots to compare RTs as estimated from lick behaviour (right) and sniff behaviour (left) for the mixture stimulus and vanillin for all where a reaction time was calculable.

178 different odors. Moreover, reaction times for vanillin were not significantly different than for the
179 mixture (licking RT: p = 0.46, paired t-test, n = 6; sniffing RT: 237 ± 45 ms, p = 0.5, unpaired t-test;
180 Figure 4J). Finally, learning in the task was likely the result of acquiring the response to the stimulus
181 rather than learning how to perceive the difference in concentration, since on the very first
182 presentation of the CS- concentration after pre-training on the CS+ concentration, mice typically
183 displayed a rapid sniffing response (Figure S5B) classically associated with novel odor identity (Roland
184 et al., 2016; Verhagen et al., 2007; Wesson et al., 2008b).

185 Thus, mice can very rapidly make decisions based on relatively modest concentration differences
186 within the timescale of a single sniff, comparing very well to their abilities in odor identity tasks
187 (Resulaj and Rinberg, 2015; Uchida and Mainen, 2003; Wesson et al., 2008b).

188 ***Variance in sniffing has no overt impact on performance in a fine concentration***
189 ***discrimination task***

190 To determine whether sniff variation impacts the concentration decisions of mice, trained mice were
191 advanced on to a 5-concentration task. Here, three new intermediate concentrations between the
192 two previously learned concentrations were presented (Figure 5A). The concentration most similar to
193 the learned CS+ was rewarded as a CS+, while the other two concentrations, including one exactly
194 halfway between the previously learned concentrations, were treated as CS- (Figure 5A). 2-3 sessions
195 of 200 trials were performed on this task, over which mice generally performed at a high level of
196 accuracy (Figure 5B-C, mean percent correct across session = 75 ± 6%, n = 8 mice). However, mice
197 displayed a graded percentage of correct versus error trials across concentrations, indicating that the
198 discrimination task was not trivial. Thus, shifts in perceived concentration should be overtly seen in
199 the performance curves.

200 Three lines of evidence suggests that sniff variance does not grossly affect concentration
201 discrimination. First, we separated trials according to whether the first sniff was fast (<30th percentile
202 inhalation duration) or slow (>70th percentile) (Figure 5D). This resulted in a comparison of trials

203 between which the difference in the inhalation duration matched or exceeded that used in the whole
204 cell recordings when comparing fast and slow sniff trials (Figure 5E). Recalculating performance curves
205 for each subset, there were no large or significant differences in the performance curves for mice
206 performing on either contingency (Figure 5F; $p>0.01$ paired t-tests). Secondly, on a small selection of
207 trials, the puff stimulus (as used during the physiological recordings) was used to evoke fast sniffs,
208 including the first inhalation (Figure 5G). The mean changes in first inhalation duration evoked by this
209 puff were again highly comparable to that used for analysis of fast and slow sniffs in the physiological
210 data (Figure 5H). While this had a minor but insignificant effect on error rate likely owing to distraction
211 (percent correct: control trials = 83 ± 8%, probe trials = 77 ± 9%, $p = 0.16$ paired t-test, n = 8 mice),
212 there were remarkably no gross differences in the performance curves compared to control trials
213 ($p>0.01$, paired t-tests; Figure 5J). Finally, when separating trials for each concentration according to
214 the response of the mouse (either 'go' or 'no go', Figure 5K), the mean difference in first inhalation
215 between go and no-go trials was significantly smaller than used in the physiological analysis (Figure
216 5L), and across different concentrations there were no large or significant differences in the first
217 inhalation duration according to the response ($p>0.01$, paired t-tests; Figure 5M).

218 Reductions of inhalation duration of 10-20 ms rendered 1% and 2.5% concentrations indiscriminable
219 within MTC responses (Figure 3E-K). Here we are comparing similar and even larger reductions in
220 inhalation duration, yet behaviourally the ability to discriminate concentration shows no dramatic
221 differences, congruent with the recent findings in rats for a different task (Shusterman et al., 2017).
222 Thus, variable sniffing appears to have no overt negative impact on concentration perception.

223 ***Mitral and tufted cells respond to inhalation changes in cell type specific ways***

224 We have so far shown that it is difficult to distinguish the effect of a change in inhalation or a change
225 in concentration via their effects on MTC responses (Figure 1-3), yet mice are perfectly capable of fine
226 concentration discrimination in the face of fluctuating inhalations (Figure 5). We thus conjecture that

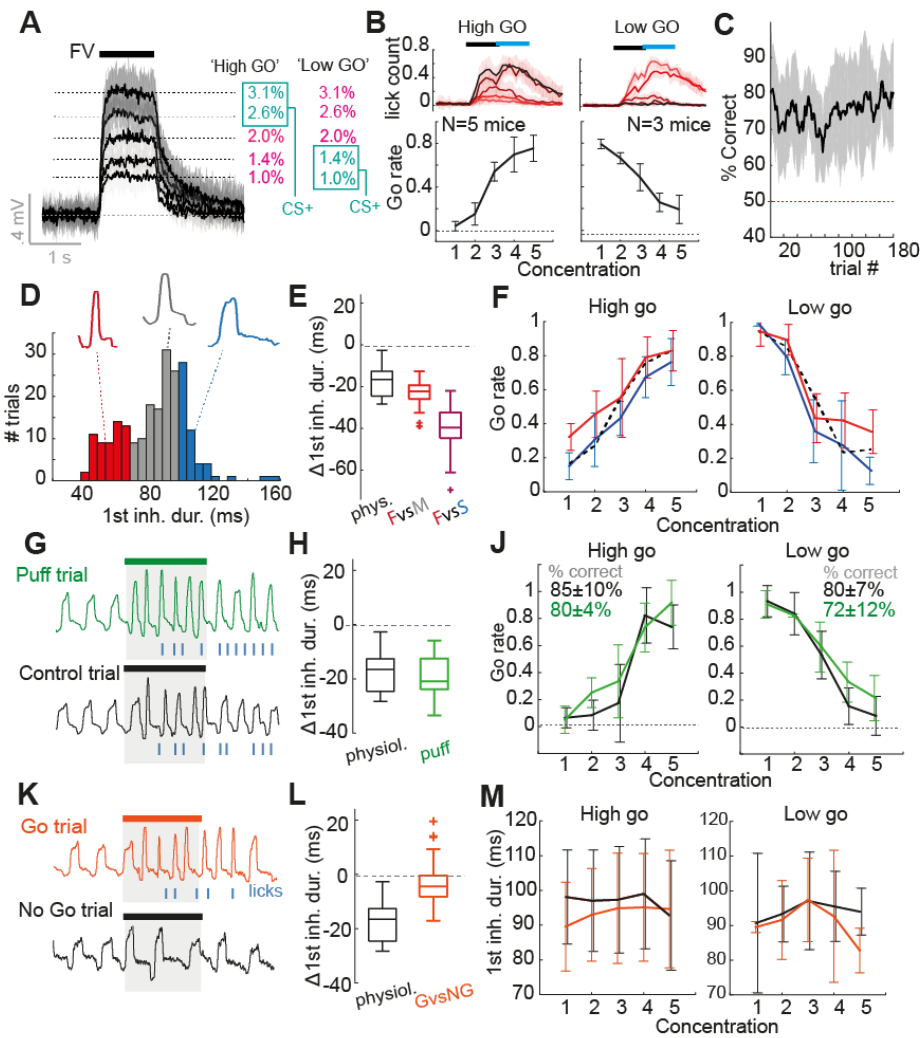

Figure 5. Variance in inhalation has no overt impact on concentration discrimination performance.

(**A**) Diagram to show average PID traces for the 5 different concentrations and contingency schemes. Shaded area shows SD. (**B**) Top: Mean lick counts averaged across mice for the 5 different concentrations (darkest = strongest) for both high go and low go contingencies. Black bar indicates odor stimulus, and blue bar indicates response period. Bottom: average go rate (percentage of trials with a go response) across mice for all 5 concentrations. (**C**) Average % correct across all sessions of the 5 concentration discrimination task (n = 3 sessions x 8 mice). Shaded area shows standard deviation. (**D**) Example histogram of inhalation durations of the first sniff during an odor stimulus across trials for one mouse. Data for each mouse is partitioned into fast inhalations (30th percentile, red), slow inhalations (>70th percentile, blue), and other (grey). Example representative nasal flow waveforms for a single sniff of each subset are shown. (**E**) Comparison of changes in the first inhalation between physiology and behavioural experiment. Black ('phys.') shows distribution of mean change used for analysis of odor responses (Figure 2-3) for 20 cell-odor pairs recorded in passive mice. Red ('FvsM') shows mean difference between red and grey sections of the inhalation distribution as in panel D for all mice and concentrations (n = 8 mice x 5 concentrations); Purple 'FvsS' shows the same as for 'FvsM', but shows mean difference between red and blue sections of the inhalation duration distribution as in panel D. *Continued on next page…*

(**F**) Go rate as a function of concentration when splitting trials according to duration of first inhalation as in D. Dotted line shows mean go rate for sniffs with inhalation between 30th and 70th percentile. (**G**) Example sniff traces for one animal for a puff trial (a trial in which an air puff to the flank was used to evoke fast sniffing) and an adjacent control trial of the same odor. (**H**) Comparison of changes in mean first inhalation duration for physiological analysis (Figure 2-3, n = 20) and for puff vs control trials during behaviour (n = 8 mice x 5 concentrations). (**J**) Mean go rate as a function of concentration across mice for puff trials (green) vs control trials (black). (**K**) Example sniff traces for one animal for a go trial and a no go trial for a given odor concentration. (**L**) General comparison of mean first inhalation change for physiological analysis (Figure 2-3), n = 20) and between go and no-go trials during behaviour (n = 8 mice x 5 concentrations). (**M**) Mean first inhalation duration for go vs no go trials across all mice in each concentration category.

the olfactory system requires information about the kind of inhalation that just occurred to infer whether concentration or sniffing evoked the response change. This could either be achieved through an efference copy of the sniffing control signal, or reafference (the sensory result of the sniff motor command). Congruent with the latter idea, OSNs have been demonstrated to respond to pressure changes (Grosmaitre et al., 2007), giving rise to sniff coupling in the olfactory bulb (Adrian, 1950; Cang and Isaacson, 2003; Fukunaga et al., 2012; Macrides and Chorover, 1972; Margrie and Schaefer, 2003), which disappears with naris occlusion (Margrie and Schaefer, 2003). We thus wanted to determine whether the olfactory bulb reports changes in single sniffs on a short timescale.

We took baseline activity in absence of odor as a proxy for the large portion of mitral and tufted cells which will not be responsive to an odor, whose activity could instead be used to directly determine the kind of sniff that took place. To do this we analysed the cellular activity of 45 MTCs recorded in passive mice across over 1000-2000 sniffs occurring in absence of the odor. Sniffs were categorised according to inhalation duration, and peristimulus time histograms and average membrane potential waveforms were calculated over 250 ms triggered by inhalation onset for each subset (Figure 6A-C). We found that individual mitral and tufted cells would show linear transformations in their activity according to the duration of the inhalation just occurring. For example, some cells showed increased spike count (Figure 6A_1-B_1) and depolarising membrane potential (Figure 6C_1) as inhalations became

245 faster, while others showed decreasing spike count (Figure $6A_2$-B_2) and more hyperpolarising
246 membrane potential (Figure $6C_2$). 24% of cells showed significant ($p<0.01$) relationships between spike
247 count and inhalation duration (Figure 6D) compared to only 3% in shuffle controls. R^2 for the actual
248 correlations were also significantly higher than for shuffle controls (actual R^2 median = 0.54, IQR=0.17-
249 0.82; shuffled median=0.18, IQR=0.04-0.45, $p=2=1x10^{-4}$, Ranksum, n=41 vs 369; Figure 6D). Similarly,
250 22% showed significant correlations with mean membrane potential compared to 2% of shuffle
251 controls (Figure 6D) ($p<0.05$, linear regression), with R^2 values for the actual data being significantly
252 higher than for shuffled data (actual R^2 median = 0.56, IQR=0.20-0.73; shuffled median=0.18,
253 IQR=0.04-0.41, $p=9x10^{-7}$, Ranksum, n=41 vs 369). Timing of activity was also often linearly correlated
254 with inhalation duration, generally with the peak of the membrane potential shifting to earlier times
255 as inhalation duration reduced (significant R values in 32% of cells vs 2% in shuffle controls (Figure
256 6D); actual R^2 median=0.50, IQR=0.22-0.86; shuffled median=0.20, IQR=0.05-0.43, $p=2x10^{-6}$).
257 Altogether 51% of cells showed a significant relationship ($p<0.01$) between inhalation duration and at
258 least one or more of these activity parameters (Figure 6E).

259 It has previously been suggested in anaesthetized animals that MCs and TCs are coupled to different
260 phases of the sniff cycle, with MCs coupled to inhalation and TCs to exhalation (Fukunaga et al., 2012),
261 a feature which is supported by recent data from the awake mouse, allowing designation of putative
262 MC and TC phenotypes based on phase preference (Jordan et al., 2017). This divergent coupling is
263 thought to be the result of divergent sniff-driven circuit architecture, with TCs largely driven by direct
264 excitation and MC activity heavily modulated in parallel via feed-forward inhibition (Fukunaga et al.
265 2012). Since cells could either depolarise or hyperpolarise as a function of inhalation duration (Figure
266 6), we wanted to test whether this could be explained by cell type. Indeed we found cases where
267 morphologically reconstructed cells showed correlations between certain activity parameters and

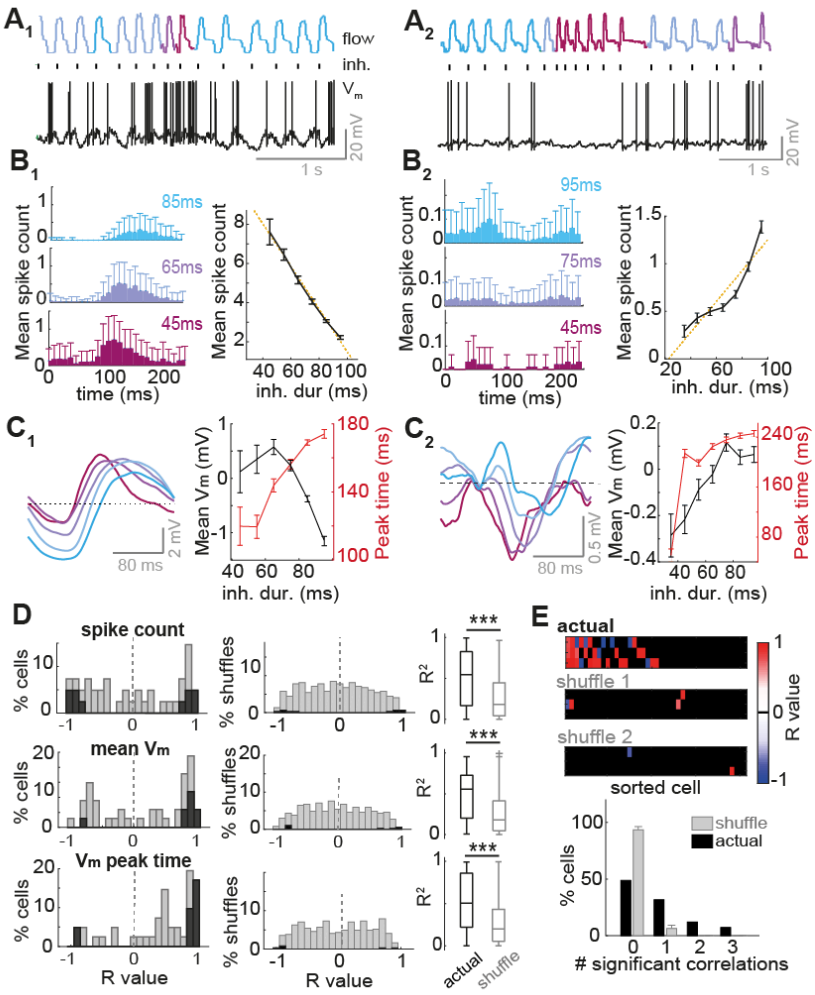

Figure 6. Inhalation duration transforms mean baseline MTC activity in a large proportion of cells.

A_1 to C_1 refer to one example cell, while A_2 to C_2 refer to a different example cell. (**A**) Example nasal flow traces and V_m traces in absence of odor. Sniffs are colour coded according to inhalation duration (blue = slow, and red = fast). Black ticks indicate inhalation onset. (**B**) Left: Average spike count triggered by inhalations of different durations (denoted on each histogram). Right: mean spike count per sniff as a function of inhalation duration. Errorbars = standard error (SE). (**C**) Left: Inhalation-triggered mean membrane potential waveforms for sniffs of different inhalation duration. Right: mean V_m and timing of V_m peak for membrane potential waveforms across all sniffs as a function of inhalation duration. Errorbars = SE. (**D**) Left: Histograms of R values for correlations between inhalation duration and different activity variables: (from top to bottom) spike count, mean membrane potential, and the timing of peak membrane potential. Middle: histograms of R values between the different activity parameters and inhalation duration for shuffle controls (n = 10 shuffles x 45 cells). Dark bars show significant correlations. Right: Boxplots show comparison of actual R^2 values for the correlations as compared to shuffle controls.

Continued on next page…

(**E**) Top: Heatmap of R values for correlations between inhalation duration and 3 different activity parameters (spike count, mean membrane potential and timing of peak membrane potential, rows 1-3 respectively), for 45 mitral and tufted cells. Cells are sorted left-right by largest number of significant correlations to lowest number. Black squares show where the correlation was insignificant ($p>0.01$, regression analysis). Two lowest heatmaps show the same data but for 2 example shuffle controls, where inhalation durations were shuffled with respect to the physiology, and the data re-analysed. This gives an indication of false positive rates in this analysis. Bottom: histogram to show proportion of cells with 0 to 3 significant correlations between the different activity parameters and inhalation duration. Grey shows proportion for shuffle controls.

inhalation duration, with polarity corresponding to cell type as predicted. For example, the tufted cell in Figure 7A_1-C_1 showed significant depolarisation as inhalation duration gets shorter (increased spike count and more depolarised V_m waveform), while the mitral cell in Figure 7A_2-D_2 showed the opposite correlation, showing increasing inhibition as inhalation duration reduced. We plotted R values for these correlations as a function of sniff cycle phase preference (calculated from subthreshold activity) for all cells showing strong correlations ($p<0.05$, $R^2>0.6$). Indeed, for both parameters (mean V_m and spike count), there was a significant organisation according to phase for both mean V_m ($p<0.01$, bootstrapping, see methods; Figure 7D) and spike count ($p<0.001$; bootstrapping, see methods; Figure 7E). Moreover, comparing R values between the phase boundaries assigned for putative MCs and TCs resulted in significant differences between the two groups in each case (mean V_m: pMC: median = 0.93, IQR = 0.84 to 0.95, n = 6; pTC: median = -0.83, IQR = -0.96 to -0.82, n = 10; p = 0.002, Ranksum; spike count: pMC: median = 0.84, IQR = -0.88 to 0.96, n = 22; pTC: median = -0.92, IQR = -0.94 to -0.89, n = 12; p = 0.008, Ranksum).

Thus, phase locking, which likely relates to MC and TC phenotype, determines how a cell will respond to changing sniff parameters in absence of odor. Thus the large population of cells that are not directly involved with the encoding of odor information could instead be utilised to encode the parameters of each inhalation.

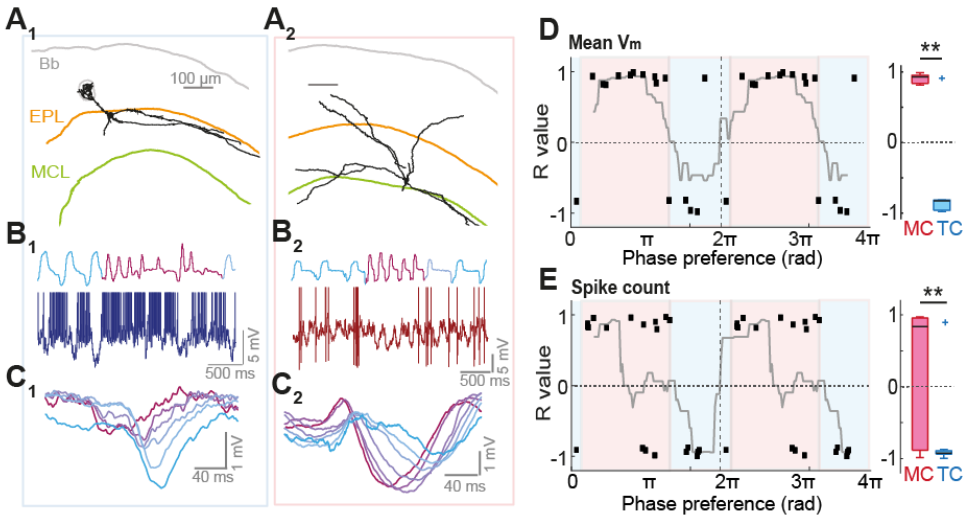

Figure 7. Cell type specificity of effect of inhalation.

(**A₁**) Reconstructed morphology of a tufted cell recorded in awake mouse. 'Bb' refers to brain border, 'EPL' refers to external plexiform layer and 'MCL' refers to mitral cell layer (these morphologies have been previously published in Jordan et al. 2017 for different purposes). (**B₁**) Example nasal flow and V_m trace during a rapid sniff bout (blue to purple represents slow to fast inhalation on flow trace. Spikes have been cropped. (**C₁**) Mean membrane potential waveform for different bands of inhalation duration: blue = long inhalation duration, purple = short. (**A₂**)-(**C₂**) as for A_1-C_1, but for a filled mitral cell recorded in an awake mouse. (**D**) R values for correlations between inhalation duration and mean V_m as a function of phase preference. Only strong correlations have been included ($p<0.05$ and $R^2>0.6$). Grey line shows mean R value for all cells within a 2 radian moving window (centred), to give an idea of the phase modulation strength of the data. Boxplots to the right compare all values within the putative MC (red) and putative TC (blue) phase boundaries. (**E**) As for panel D, but for mean spike count per sniff.

286

287 ***Inhalation change can be detected and decoded from MTC spiking on rapid timescales***

288 We next sought to determine whether we could read out changes in inhalation from the spiking
289 activity of cells in absence of odor, as a proxy for cells that are not responding directly to the odor.

290 We first wanted to determine how rapidly a change in inhalation could be detected. For all cells with
291 enough sniff variation (>50 sniffs in each inhalation duration category), we calculated sequences of
292 spike histograms for different inhalation durations using random subsets of sniffs within each group
293 (Figure 8A; see methods). We constructed either a sequence with PSTHs calculated from three

294 consecutive sniffs of 95 ms inhalation duration, or a sequence with PSTHs calculated from 2
295 consecutive sniffs of 95 ms, with the last PSTH instead constructed from 55 ms inhalation duration
296 sniffs (Figure 8A). Using these, it was possible to determine a change in inhalation duration (95 to 55
297 ms inhalation duration) within only 70 ± 12ms by calculating Euclidean distances for constructed
298 population vectors of the two different sequences (Figure 8B see methods). Smaller changes in
299 inhalation duration (95 to 75 ms) could also be detected on similarly rapid timescales (Figure S6).

300 We next investigated whether the population activity of multiple mitral and tufted cells provides
301 sufficient information for reliable detection of individual sniff cycles with fast and slow inhalation
302 speeds. From 42 single-cell recordings of mitral and tufted cell activity, we constructed an emulated
303 population spiking matrix for respiration cycles for fast (37-80 ms) and slow (96-183 ms) inhalations.
304 After training synaptic weights from all the 42 neurons and an activation threshold, a single output
305 neuron could achieve perfect detection performance of cycles with fast and slow inhalations (Figure
306 8C see methods). Reliable discrimination (Matthews correlation coefficient of 0.90) of individual fast
307 and slow inhalation cycles could be achieved within 130 ms after inhalation onset (Figure 8D).

308 Thus, even for relatively low numbers of neurons, mitral and tufted cell activity - in absence of odor
309 input - is informative of the inhalation that just occurred, such that non-odor responsive cells could
310 be utilised by the olfactory system to distinguish sniff changes versus concentration changes.

311 Discussion

312 For stable perception, sensory systems must find ways of encoding of stimulus features across a range
313 of conditions. Here we show that faster sniffs can evoke response changes in the olfactory bulb that
314 appear indistinguishable from those caused by increasing concentration (Figure 1-3), yet mice are
315 highly capable of perceiving concentration on fast timescales, regardless of sniffing parameters (Figure
316 4-5). We reason that the only way the olfactory system can distinguish these two occurrences is via
317 information about the kind of sniff that just occurred. This could potentially be achieved through
318 corollary discharge from a motor circuit involved with breathing rhythms (such as the pre-bötzinger

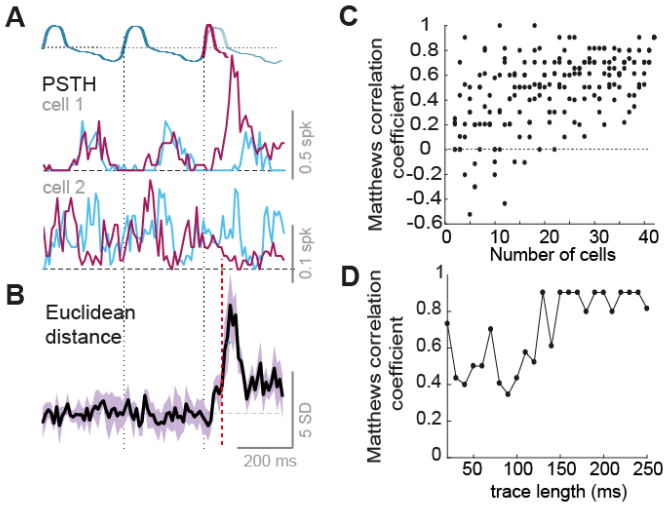

Figure 8. MTC spiking activity is informative of the type of inhalation occurring

(**A**) Top: diagram to show construction of sniff sequences of different inhalation duration: either three of 95 ms inhalation duration, or two of 95 ms with the final sniff of 55 ms duration. Below: two example PSTH sequences averages from random subsets of sniffs that show the particular inhalation duration. Blue line shows the PSTH sequence for 4 sniffs of 95 ms, and purple show sequence in which the last inhalation is of 55ms. (**B**) Mean Euclidean distance calculated between population vectors constructed from the two sniff sequences as in panel A. Plot shows the average of 5 different subsets of data, and shaded area shows standard deviation. Dashed red line indicates time of significant detection of change. (**C**) Classification performance of a trained neural network for distinction of fast and slow inhalations from the emulated population spiking activity constructed from different numbers of MTCs (see methods for details). (**D**) Classification performance for distinction of fast and slow inhalations for the full 42 MTC spiking dataset as a function of the time since inhalation onset.

complex). However we find that single MTC activity already correlates with inhalation duration (Figure 6), and that this is likely generated from feed-forward input in a cell type specific way (Figure 7), allowing inference about the kind of sniff that just occurred on a rapid timescale (Figure 8). Thus, the olfactory bulb itself does not appear to be the site where the sniff-invariant percept of intensity is generated, but does appear to already contain the information needed to generate the percept elsewhere.

Given the timescale of decision making for concentration (Figure 4), it seems likely that the information used by the mouse is the fast timescale temporal shifts in excitation that have been

328 previously described (Cang and Isaacson, 2003; Fukunaga et al., 2012; Sirotin et al., 2015).
329 Congruently, this temporal information contributes to the entirety of concentration discriminability
330 on such a timescale in our dataset (Figure 3E). It has been suggested that high baseline firing rates of
331 MTCs could obscure such a latency code for concentration being used (Mainland et al., 2014), however
332 this was based on a high estimation of baseline FRs from unit recordings. The whole cell recordings
333 we employ here are thought to be unbiased in terms of baseline FRs (Kollo et al., 2014; Margrie et al.,
334 2002; Shoham et al., 2006), and discriminability of MTC responses based on latency shifts is overt
335 (Figure 3E). Congruently it is known that mice can perceive the latency difference in optogenetic
336 glomerular activation on the order of tens of milliseconds (Rebello et al., 2014; Smear et al., 2013).

337 Sniff changes have been hypothesized to alter odor concentration profiles within the nasal cavity
338 (Shusterman et al., 2017; Teghtsoonian et al., 1978). Here we show for the first time directly that sniff
339 changes can indeed mimic the effect of concentration change at the level of both firing rates (Figure
340 1), and temporal shifts in spike activity (Figure 2-3). This is not to say that OSN input is perfectly
341 matched when we compare faster sniff rates and higher concentration. In fact, since subthreshold
342 inhibition is greater for the higher concentration, it would appear that the input strength is higher for
343 the case of increased concentration as compared to faster sniffing. Despite this, overt changes in the
344 spiking output are very similar for increased sniff frequency as compared to increased concentration.
345 Potentially, inhibitory circuits are normalising the spiking output across large changes in input (within
346 a dynamic range), such that while we see differences in subthreshold inhibition, the excitatory spike
347 outputs look very similar. Such a role has been suggested for periglomerular neurons (Roland et al.,
348 2016) and parvalbumin positive interneurons in the external plexiform layer (Kato et al., 2013;
349 Miyamichi et al., 2013).

350 It has been known for some time that the olfactory bulb is highly modulated by the sniff cycle (Adrian,
351 1950; Cang and Isaacson, 2003; Fukunaga et al., 2012; Macrides and Chorover, 1972; Margrie and
352 Schaefer, 2003). Since sniff modulation is more overt in anaesthetized mice and is reduced at higher

353 sniff frequencies (Bathellier et al., 2008; Carey and Wachowiak, 2011; Kay and Laurent, 1999), the
354 importance of sniff modulation in the awake animal may come into question. Here we find that sniff
355 patterning of activity gives rise to linear transformations of baseline activity as inhalation parameters
356 are changed, a feature which is widespread throughout MTCs (Figure 6). We thus reason that a
357 primary function of sniff modulation is to inform the olfactory system of what kind of inhalation took
358 place, such that a change in concentration and a change in sniffing are distinguishable. Congruently
359 we find that inhalation parameters can indeed be readily and rapidly inferred from the spiking activity
360 of MTCs (Figure 8).

361 Encoding of 'sniff effort' has been hypothesized previously when psychophysics showed that humans
362 could categorise concentrations well despite large changes in inhalation flow rate (Teghtsoonian et
363 al., 1978). Airway resistance is subject to continual changes, and even differs between the two nostrils
364 (Principato and Ozenberger, 1970; Sobel et al., 1999), which will naturally result in varying nasal flow
365 rates for identical respiratory motor commands. Previous work has shown that sniff modulation of the
366 olfactory bulb is generated peripherally rather than centrally, since blocking the naris abolishes sniff
367 modulation in the olfactory bulb (Margrie and Schaefer 2003). Thus reafference using mechanoceptive
368 encoding of sniff pressure, rather than efference copy of the motor commands (which would require
369 constantly updated internal models to calculate the effect on airway flow for each nostril) may be the
370 optimal strategy for encoding inhalation parameters. This could be the reason that olfactory receptors
371 evolved to respond to pressure changes as well as olfactory stimuli (Connelly et al., 2015; Grosmaitre
372 et al., 2007), and indeed may comprise a feature rather than a bug in the olfactory system.
373 Consistently, concentration perception in humans can be affected when the nostril flow rate was
374 changed via experimenter-induced changes in airway resistance instead of volitional changes in sniff
375 pressure (Teghtsoonian and Teghtsoonian, 1984) – i.e. only when flow rate is altered but pressure
376 stays constant. Moreover, imaging of the olfactory cortex in humans identified a region which
377 primarily responds to the sensory effect of sniffing in absence of odor (Sobel et al., 1998).

378 An accompanying study intuitively suggests that the advance of odor-driven excitation as sniff
379 frequency increases is the result of fluid dynamics in the nasal cavity (Shusterman et al., 2017). A large
380 fraction of our cells show an advance of their baseline activity peak as the inhalation becomes faster
381 (Figure 6D). We could thus hypothesise that non-odor responsive MTCs within a region of the bulb
382 can provide information about the timing of inspired air reaching the epithelium. If the inhalation
383 becomes faster, both responsive and the much larger population of unresponsive cells show a latency
384 reduction in their peak activity, while if concentration has increased, only the sparse odor responsive
385 population will show this latency shift. Thus, a relative timing code could be used as a sniff-invariant
386 representation of concentration (Figure S8). Exactly where and how the two kinds of information could
387 be integrated to form a sniff invariant representation of concentration should be the objective of
388 future investigations, though recent evidence from the piriform cortex of awake mice already suggests
389 that cortical interneurons sharpen the latency shifts evoked by concentration change and encode
390 concentration via the synchronicity of ensemble firing (Bolding and Franks, 2017). It is also possible
391 that in a mouse performing a concentration guided task, olfactory bulb physiology could be altered by
392 top-down circuits in such a way as to generate a sniff invariant representation of concentration using
393 information about the sniff dynamics.

394 It is possible that at much larger sample sizes of cells than reported here, a small subpopulation of
395 neurons capable of reporting concentration invariant across sniffs become detectable. It is also
396 possible that we have missed activity parameters at the population level, such as spike synchrony,
397 which could conceivably be more stable reporters of concentration in the face of fluctuating sniffs.
398 We deem these confounds less likely since a complimentary unit recording study finds that the latency
399 shift of excitatory response due to sniff change is widespread throughout a larger sample of MTCs
400 (Shusterman et al., 2017).

401 In conclusion, effective concentration in the naris can either be self-generated through changes in
402 sniffing, or the consequence of a true change in environmental concentration, yet mice can perform

403 sniff-invariant concentration discrimination. The olfactory bulb contains information about both the
404 odor concentration alongside the inhalation dynamics, which together may allow inference about
405 whether a sniff change or a concentration change occurred, overall enabling sniff-invariant
406 concentration perception.

407 Author Contributions

408 A.T.S., and R.J., designed all experiments, R.J. performed all experiments, and analysed all data apart
409 from the discriminability of fast and slow sniffs (Figure 8C-D), which was performed by M.K. The article
410 was written by R.J. and M.K. with contributions from A.T.S. The authors declare no competing financial
411 interests.

412 Acknowledgments

413 We thank Martyn Stopps and Nicholas Burczyk for assistance with custom made equipment, Mostafa
414 Nashaat and Edward Bracey for initial support with behavioral training, Christoph Schmidt-Hieber for
415 advice on whole-cell recording *in vivo*, and Roma Shusterman, Andrew Erskine, Christina Marin and
416 Kevin Bolding for helpful comments on the manuscript. This work was supported by the Francis Crick
417 Institute which receives its core funding from Cancer Research UK (FC001153), the UK Medical
418 Research Council (FC001153), and the Wellcome Trust (FC001153); by the UK Medical Research
419 Council (grant reference MC_UP_1202/5); by the DFG (SPP 1392); and a Boehringer Ingelheim Fonds
420 PhD fellowship to RJ. AS is a Wellcome Trust Investigator (110174/Z/15/Z).

421 References

422 Abraham, N.M., Spors, H., Carleton, A., Margrie, T.W., Kuner, T., and Schaefer, A.T. (2004).
423 Maintaining accuracy at the expense of speed: stimulus similarity defines odor discrimination time in
424 mice. Neuron *44*, 865–876.

425 Adrian, E.D. (1950). The electrical activity of the mammalian olfactory bulb. Electroencephalogr. Clin.
426 Neurophysiol. *2*, 377–388.

427 Bathellier, B., Buhl, D.L., Accolla, R., and Carleton, A. (2008). Dynamic ensemble odor coding in the
428 mammalian olfactory bulb: sensory information at different timescales. Neuron *57*, 586–598.

429 Bolding, K.A., and Franks, K.M. (2017). Complementary codes for odor identity and intensity in
430 olfactory cortex. eLife *6*, e22630.

Cang, J., and Isaacson, J.S. (2003). In vivo whole-cell recording of odor-evoked synaptic transmission in the rat olfactory bulb. J. Neurosci. Off. J. Soc. Neurosci. *23*, 4108–4116.

Carey, R.M., and Wachowiak, M. (2011). Effect of sniffing on the temporal structure of mitral/tufted cell output from the olfactory bulb. J. Neurosci. Off. J. Soc. Neurosci. *31*, 10615–10626.

Cleland, T.A., Chen, S.-Y.T., Hozer, K.W., Ukatu, H.N., Wong, K.J., and Zheng, F. (2012). Sequential mechanisms underlying concentration invariance in biological olfaction. Front. Neuroengineering *4*.

Connelly, T., Yu, Y., Grosmaitre, X., Wang, J., Santarelli, L.C., Savigner, A., Qiao, X., Wang, Z., Storm, D.R., and Ma, M. (2015). G protein-coupled odorant receptors underlie mechanosensitivity in mammalian olfactory sensory neurons. Proc. Natl. Acad. Sci. *112*, 590–595.

Cury, K.M., and Uchida, N. (2010). Robust Odor Coding via Inhalation-Coupled Transient Activity in the Mammalian Olfactory Bulb. Neuron *68*, 570–585.

Frasnelli, J., Hummel, T., Berg, J., Huang, G., and Doty, R.L. (2011). Intranasal Localizability of Odorants: Influence of Stimulus Volume. Chem. Senses *36*, 405–410.

Fukunaga, I., Berning, M., Kollo, M., Schmaltz, A., and Schaefer, A.T. (2012). Two Distinct Channels of Olfactory Bulb Output. Neuron *75*, 320–329.

Ghatpande, A.S., and Reisert, J. (2011). Olfactory receptor neuron responses coding for rapid odour sampling. J. Physiol. *589*, 2261–2273.

Grosmaitre, X., Santarelli, L.C., Tan, J., Luo, M., and Ma, M. (2007). Dual functions of mammalian olfactory sensory neurons as odor detectors and mechanical sensors. Nat. Neurosci. *10*, 348–354.

Helmholtz, H. von (1867). Handbuch der physiologischen Optik (Leipzig : Leopold Voss).

Jordan, R., Fukunaga, I., Kollo, M., and Schaefer, A.T. (2017). Active sampling state dynamically enhances olfactory bulb odor representation. bioRxiv 222588.

Kato, H.K., Gillet, S.N., Peters, A.J., Isaacson, J.S., and Komiyama, T. (2013). Parvalbumin-expressing interneurons linearly control olfactory bulb output. Neuron *80*, 1218–1231.

Kay, L.M., and Laurent, G. (1999). Odor- and context-dependent modulation of mitral cell activity in behaving rats. Nat. Neurosci. *2*, 1003–1009.

Kepecs, A., Uchida, N., and Mainen, Z.F. (2007). Rapid and precise control of sniffing during olfactory discrimination in rats. J. Neurophysiol. *98*, 205–213.

Kollo, M., Schmaltz, A., Abdelhamid, M., Fukunaga, I., and Schaefer, A.T. (2014). “Silent” mitral cells dominate odor responses in the olfactory bulb of awake mice. Nat. Neurosci. *17*, 1313–1315.

Macrides, F., and Chorover, S.L. (1972). Olfactory bulb units: activity correlated with inhalation cycles and odor quality. Science *175*, 84–87.

Mainland, J., and Sobel, N. (2006). The Sniff Is Part of the Olfactory Percept. Chem. Senses *31*, 181–196.

Mainland, J.D., Lundström, J.N., Reisert, J., and Lowe, G. (2014). From Molecule to Mind: an Integrative Perspective on Odor Intensity. Trends Neurosci. *37*, 443–454.

Margrie, T.W., and Schaefer, A.T. (2003). Theta oscillation coupled spike latencies yield computational vigour in a mammalian sensory system. J. Physiol. *546*, 363–374.

Margrie, T.W., Brecht, M., and Sakmann, B. (2002). In vivo, low-resistance, whole-cell recordings from neurons in the anaesthetized and awake mammalian brain. Pflugers Arch. *444*, 491–498.

Meredith, M. (1986). Patterned response to odor in mammalian olfactory bulb: the influence of intensity. J. Neurophysiol. *56*, 572–597.

Miyamichi, K., Shlomai-Fuchs, Y., Shu, M., Weissbourd, B.C., Luo, L., and Mizrahi, A. (2013). Dissecting local circuits: parvalbumin interneurons underlie broad feedback control of olfactory bulb output. Neuron *80*, 1232–1245.

Parthasarathy, K., and Bhalla, U.S. (2013). Laterality and symmetry in rat olfactory behavior and in physiology of olfactory input. J. Neurosci. Off. J. Soc. Neurosci. *33*, 5750–5760.

Principato, J.J., and Ozenberger, J.M. (1970). Cyclical changes in nasal resistance. Arch. Otolaryngol. Chic. Ill 1960 *91*, 71–77.

Rebello, M.R., McTavish, T.S., Willhite, D.C., Short, S.M., Shepherd, G.M., and Verhagen, J.V. (2014). Perception of Odors Linked to Precise Timing in the Olfactory System. PLOS Biol. *12*, e1002021.

Resulaj, A., and Rinberg, D. (2015). Novel Behavioral Paradigm Reveals Lower Temporal Limits on Mouse Olfactory Decisions. J. Neurosci. *35*, 11667–11673.

Roland, B., Jordan, R., Sosulski, D.L., Diodato, A., Fukunaga, I., Wickersham, I., Franks, K.M., Schaefer, A.T., and Fleischmann, A. (2016). Massive normalization of olfactory bulb output in mice with a “monoclonal nose.” eLife *5*, e16335.

Rospars, J.P., Lánský, P., Duchamp-Viret, P., and Duchamp, A. (2000). Spiking frequency versus odorant concentration in olfactory receptor neurons. Biosystems *58*, 133–141.

Rubin, B.D., and Katz, L.C. (1999). Optical imaging of odorant representations in the mammalian olfactory bulb. Neuron *23*, 499–511.

Shoham, S., O’Connor, D.H., and Segev, R. (2006). How silent is the brain: is there a “dark matter” problem in neuroscience? J. Comp. Physiol. A Neuroethol. Sens. Neural. Behav. Physiol. *192*, 777–784.

Shusterman, R., Sirotin, Y.B., Smear, M.C., Ahmadian, Y., and Rinberg, D. (2017). Sniff invariant odor coding. bioRxiv 174417.

Sirotin, Y.B., Shusterman, R., and Rinberg, D. (2015). Neural Coding of Perceived Odor Intensity,,. eNeuro *2*.

Slotnick, B.M., and Ptak, J.E. (1977). Olfactory intensity-difference thresholds in rats and humans. Physiol. Behav. *19*, 795–802.

Smear, M., Resulaj, A., Zhang, J., Bozza, T., and Rinberg, D. (2013). Multiple perceptible signals from a single olfactory glomerulus. Nat. Neurosci. *16*, 1687–1691.

Sobel, N., Prabhakaran, V., Desmond, J.E., Glover, G.H., Goode, R.L., Sullivan, E.V., and Gabrieli, J.D. (1998). Sniffing and smelling: separate subsystems in the human olfactory cortex. Nature *392*, 282–286.

Sobel, N., Khan, R.M., Saltman, A., Sullivan, E.V., and Gabrieli, J.D. (1999). The world smells different to each nostril. Nature *402*, 35.

Spors, H., and Grinvald, A. (2002). Spatio-temporal dynamics of odor representations in the mammalian olfactory bulb. Neuron *34*, 301–315.

Teghtsoonian, R., and Teghtsoonian, M. (1984). Testing a perceptual constancy model for odor strength: the effects of sniff pressure and resistance to sniffing. Perception *13*, 743–752.

Teghtsoonian, R., Teghtsoonian, M., Berglund, B., and Berglund, U. (1978). Invariance of odor strength with sniff vigor: an olfactory analogue to size constancy. J. Exp. Psychol. Hum. Percept. Perform. *4*, 144–152.

Uchida, N., and Mainen, Z.F. (2003). Speed and accuracy of olfactory discrimination in the rat. Nat. Neurosci. *6*, 1224–1229.

Uchida, N., and Mainen, Z.F. (2008). Odor Concentration Invariance by Chemical Ratio Coding. Front. Syst. Neurosci. *1*.

Verhagen, J.V., Wesson, D.W., Netoff, T.I., White, J.A., and Wachowiak, M. (2007). Sniffing controls an adaptive filter of sensory input to the olfactory bulb. Nat. Neurosci. *10*, 631–639.

Wachowiak, M. (2011). All in a sniff: olfaction as a model for active sensing. Neuron *71*, 962–973.

Wachowiak, M., Cohen, L.B., and Zochowski, M.R. (2002). Distributed and concentration-invariant spatial representations of odorants by receptor neuron input to the turtle olfactory bulb. J. Neurophysiol. *87*, 1035–1045.

Welker, W.I. (1964). Analysis of Sniffing of the Albino Rat 1). Behaviour *22*, 223–244.

Wesson, D.W., Donahou, T.N., Johnson, M.O., and Wachowiak, M. (2008a). Sniffing behavior of mice during performance in odor-guided tasks. Chem. Senses *33*, 581–596.

Wesson, D.W., Carey, R.M., Verhagen, J.V., and Wachowiak, M. (2008b). Rapid encoding and perception of novel odors in the rat. PLoS Biol. *6*, e82.

Wesson, D.W., Verhagen, J.V., and Wachowiak, M. (2009). Why Sniff Fast? The Relationship Between Sniff Frequency, Odor Discrimination, and Receptor Neuron Activation in the Rat. J. Neurophysiol. *101*, 1089–1102.

Wilson, C.D., Serrano, G.O., Koulakov, A.A., and Rinberg, D. (2017). Concentration invariant odor coding. bioRxiv 125039.

Wojcik, P.T., and Sirotin, Y.B. (2014). Single scale for odor intensity in rat olfaction. Curr. Biol. CB *24*, 568–573.

Youngentob, S.L., Mozell, M.M., Sheehe, P.R., and Hornung, D.E. (1987). A quantitative analysis of sniffing strategies in rats performing odor detection tasks. Physiol. Behav. *41*, 59–69.

Methods

All animal experiments were approved by the local ethics panel of the Francis Crick Institute and UK Home Office under the Animals (Scientific Procedures) Act 1986. All mice used were C57BL/6 Jax males

541 aged between 5 and 12 weeks and were obtained by in-house breeding. All chemicals were obtained
542 from Sigma Aldrich (Missouri, USA).

543 *Olfactometry*

544 Odorants were delivered to the animal using a custom made olfactometer as used previously (Kollo et
545 al., 2014; Jordan et al., 2017). This consisted of 8 different odor channels connecting two manifolds, a
546 clean air channel, and a final dilution channel carrying clean air. Air was pressure controlled at 1 Mbar
547 with a pressure regulator (IR 1000, SMC Pneumatics, California, USA). Flow was computer controlled
548 to each manifold such that the channel supplying the mouse provided a constant flow of 2000 sccm/N_2
549 at all times, meaning that no change in flow accompanied odor pulses. Odor pulses were calibrated to
550 square pulses of different concentrations using a mini photo-ionisation detector (miniPID, Aurora
551 Scientific): briefly, pure odor was presented to the PID from an open bottle, and the maximum
552 recorded voltage (V_{max}) was assumed to represent 100% saturated vapor pressure. The pulse
553 amplitudes were then calibrated according to this value, such that a given concentration C (%
554 saturated vapor pressure) could be specified by attaining a square pulse of amplitude equal to
555 $C*V_{max}/100$. Valves and flow controllers were controlled using custom-written LabView software.
556 Odors applied to animals included 2 different odor mixtures (for recordings, either mixture A: Methyl
557 salicylate, eugenol, cinnamaldehyde, creosol and 1-nonanol; or mixture B: guaiacol, valeric acid, (+)-
558 carvone, 2-phenyl ethanol and 4-allylanisol). The components of each mixture were of similar vapor
559 pressure and proportions were adjusted according to relative vapor pressure values as previously
560 (Jordan et al., 2017). For behavior, either mixture A or pure vanillin odor were applied at various
561 concentrations (Figure 4 and 5).

562 *Surgery*

563 Sterile surgical technique was applied during all surgeries. For implantation of the head-plate, mice
564 were anaesthetized with isoflurane in 95% oxygen (5% for induction, 1.5-3% for maintenance). Local
565 (mepivicaine, 0.5% s.c.) and general analgesics (carprofen 5 mg/kg s.c.) were applied immediately at

566 the onset of surgery. An incision was made dorsally above the cranium overlying the cortex and
567 cerebellum, and periosteal tissue was removed. The surface of the bone was drilled away across the
568 implantation surface using a dental drill, and cyanoacrylate was applied to the sutures between the
569 cranial bones to reduce movement. A stainless steel custom head-plate was then glued to the bone
570 surface with cyanoacrylate, and dental cement was used to reinforce the bond. For mice going on to
571 whole cell recording, an additional chamber was constructed on the bone overlying the right olfactory
572 bulb using dental cement. After surgery, the mice were allowed to recover for 48 hours with access to
573 wet diet.

574 *Whole cell recordings*

575 On the day of recording, mice were again anaesthetized with isoflurane as above, and carprofen
576 analgesic injected (5 mg/kg s.c.). A 1 mm craniotomy was made overlying the right olfactory bulb, and
577 the dura removed. A layer of 4% low melting point agar was then applied to the surface of the bulb,
578 about 0.5-1 mm deep to reduce brain movement. Cortex buffer (125 mM NaCl, 5 mM KCl, 10 mM
579 HEPES, 2 mM $MgSO_4$, 2 mM $CaCl_2$, 10 mM glucose) was used to fill the recording chamber. The animal
580 would then be transferred to the recording rig, and allowed to awake from anaesthesia for 20 minutes.
581 Whole-cell recordings were then made blindly by descending a 5-7 MΩ borosilicate glass micropipette
582 (Hilgenberg, Malsfeld, Germany) filled with intracellular solution (130 mM $KMeSO_4$, 10 mM HEPES, 7
583 mM KCl, 2 mM ATP-Na, 2 mM ATP-Mg, 0.5 mM GTP, 0.05 mM EGTA, and in some cases 10 mM
584 biocytin; pH adjusted to 7.4 with KOH, osmolarity=280 mOsm) through the agar and 180 µm into the
585 olfactory bulb with high pressure. Here pressure was reduced, and the micropipette advanced in steps
586 of 2 µm until a substantial and sudden increase in resistance was observed indicating proximity to a
587 cell. Pressure was then dropped to zero or below, and a gigaohm seal attained. Whole-cell
588 configuration was then achieved, and the membrane voltage recording made in current clamp mode.
589 Identification of mitral and tufted cells was made using electrophysiological parameters, such as in
590 input resistance below 150 MΩ, a resting membrane potential between -60 and -40 mV, and an after-

591 hyperpolarisation waveform conforming to MTC phenotype in an independent component analysis
592 performed as previously (Kollo et al., 2014; Jordan et al., 2017).

593 Altogether 14 cells were recorded in passive mice and presented with 2 different odor concentrations,
594 as well as puff stimuli to evoke fast sniffing (Figure 1 and 3). Some cells were presented two different
595 odor stimuli (two different mixtures), such that there were 20 cell-odor pairs in total. Concentrations
596 were presented in a pseudorandom order and puff stimuli occurred on a random subset of trials only
597 for the low concentration. Puff stimuli were applied simultaneous with the odor stimuli with a gentle
598 clean air stream to the flank. For some analyses, e.g. Figure 2 and for Figures 6-8, data was
599 supplemented with previously recorded cells from the passive mouse (Jordan et al., 2017) presented
600 the same odor mixtures at 1% vapor pressure (n=6 and n=38 respectively).

601 *Behavioral task and training*

602 On day 0 (48 hours after surgery), mice with head-plates implanted would begin water restriction. On
603 day 1, mice were habituated to the experimenter and hand-fed 0.5 ml of highly diluted sweetened
604 condensed milk with a Pasteur pipette. On day 2, mice were habituated to head-fixation: mice were
605 head-fixed above a treadmill and allowed access to free reward upon licking. On day 3, successfully
606 habituated mice underwent operant conditioning with repeated presentations of CS+ concentration
607 of the odor mixture until the mouse learned to lick in the 1 s after odor offset to receive the reward.
608 On day 5, the CS- concentration was also presented alongside the CS+ concentration in a
609 pseudorandom order, until the mice learned to refrain from licking to the CS-. Licking to the CS- would
610 evoke an addition of 6 s to the inter trial interval. 5 mice were trained with high concentration stimuli
611 as the CS+ ('high go'), and 3 mice were trained on the reverse contingency ('low go'). On day 6-8, mice
612 would be presented with 5 different concentrations (3 additional concentrations spanning the range
613 between the previously two learned concentrations), and contingencies as depicted in Figure 5A. On
614 day 9, five mice went on to a final session: after observing criterion performance on the binary odor
615 concentration task with the mixture as learned previously, the odor would switch to vanillin with the

616 same contingency between concentrations. Mice were carefully monitored to maintain their body-
617 weights above 80% of their pre-restriction weight and were ensured a minimum of 1 ml water per day
618 regardless of performance.

619 *Data analysis*

620 *Statistics*

621 In all cases, 5-95% confidence intervals were used to determine significance unless otherwise stated.
622 In all figures, a single asterisk denotes $p<0.05$, double asterisk denotes $p<0.01$ and a triple asterisk
623 denotes $p<0.001$. Means and error bars showing a single standard deviation either side are used in all
624 cases for normally distributed data of equal variance. Two-sided Student's t-tests were used for
625 comparison of means and Bartlett tests used to compare variances, unless otherwise stated. Boxplots
626 are used to represent any other data (data comparisons of unequal variance, or non-normally
627 distributed data), where median is plotted as a line within a box formed from 25th (q1) and 75th (q3)
628 percentile. Points are drawn as outliers if they are larger than q3 + 1.5 x (q3 - q1) or smaller than q1 –
629 1.5 x (q3 - q1). For such data, Ranksum tests were used to compare the medians, and Browne-Forsythe
630 tests used to compare variance, unless otherwise stated.

631 *Sniff parameters*

632 Using the recording of nasal flow, different sniff parameters could be extracted. First, inhalation peaks
633 were detected using Spike2 algorithms that mark each peak above a certain threshold voltage
634 manually defined by the user, such that all inhalations were included and no false positives were
635 present. Inhalation onset was defined as the nearest time-point prior to inhalation peak at which the
636 flow trace reached zero. Inhalation offset was similarly calculated as the first time point after
637 inhalation peak where the flow trace reached zero. Inhalation duration was defined as the difference
638 in time between inhalation onset and offset. Peak inhalation slopes were calculated by detecting the
639 peak value of the flow waveform differential 50-0 ms prior to inhalation peak. Sniff duration was

640 calculated as the time between subsequent inhalation onsets. Sniff frequency was calculated by taking
641 the inverse of the mean sniff duration within the odor time period.

642 *Spike rate responses and onsets*

643 Long timescale (Figure 1): for each cell, mean spike count was calculated in 250 ms time bins for the
644 full 2 s odor stimulus. These were then averaged across trials to generate PSTHs for low concentration
645 and fast sniffing (5 trials of lowest mean inhalation duration), low concentration and slow sniffing (5
646 trials with highest mean inhalation duration) and high concentration and slow sniffing. Values were
647 quadrupled to estimate FR in Hz.

648 Short timescale (Figure 2-3): for each cell, spike counts were calculated in 10 ms time bins for only the
649 first 250 ms from odor onset (aligned to first inhalation onset). These spike counts were then averaged
650 across trials for low concentration and fast inhalation (>70th percentile peak inhalation slope), low
651 concentration and slow inhalation (<30th percentile inhalation slope) and high concentration and slow
652 inhalation (<30th percentile). Onset for excitatory responses was defined at the point the mean spike
653 count exceeded the mean + 2 SDs of the baseline spike rate in the 250 ms prior to odor onset, and
654 remained there for at least 2 consecutive points.

655 *V_m responses*

656 To analyse subthreshold responses in absence of spiking activity, spikes and their AHPs were
657 subtracted from the trace. This was done by first using the 'wavemark' tool in Spike2 to detect spikes
658 by thresholding and matching them to a generated spike waveform template. The length of this spike
659 waveform template was manually adjusted for each cell according to its AHP length, but was usually
660 around -4ms to 20-30 ms post spike peak. A trace was then generated containing all detected spike
661 waveforms connected by zero values, and this was subtracted from the original voltage trace.

662 *Correlations between response changes due to sniffing and concentration change*

663 For both long and short timescale mean FR responses, changes in FR response were calculated for
664 sniff change (fast-slow sniffing, low concentration odor) and concentration change (high-low

665 concentration, slow sniffing). For all cell-odor pairs across the sample, a single regression was made
666 between FR changes for sniff change and FR changes for concentration change in the corresponding
667 time bins, generating an actual R and p value (Figure 1E and 3C). For shuffle controls, low
668 concentration trials were shuffled in respect to the sniff behaviour on each trial, and the same analysis
669 was repeated 100 times.

670 *Euclidean distance analysis of concentration discriminabilty*

671 In reference to Figure 3E and S5G: Euclidean distance was taken across the population between mean
672 spike counts for high concentration and low concentration (slow inhalation). This generated a measure
673 of discriminability between concentrations when the inhalation was slow for both concentrations. To
674 test how much of the discriminability was due to latency shift of excitation, responses which
675 underwent a detectable latency shift between high and low concentrations had their spike count
676 response to low concentration manually shifted forward according to the latency shift occurring
677 between high and low concentration. Euclidean distance was then recalculated between spike counts
678 for high concentration and the latency-shifted spike counts at low concentration. Finally, Euclidean
679 distances were taken between spike counts for high concentration (slow inhalation) and low
680 concentration (fast inhalation). Time for discrimination was calculated, if possible, as the point at
681 which the Euclidean distance exceeded the mean + 2 SDs of the baseline Euclidean distance (250 ms
682 prior to odor onset) for at least 2 consecutive 10ms time bins.

683 *Baseline activity correlations with inhalation duration*

684 For each cell (n = 48), 1000-2000 sniffs were analysed in absence of odor. Sniffs were categorised
685 according to their inhalation duration, 35-45 ms, 45-55 ms, 55-65 ms and so forth. For each individual
686 sniff, different parameters were calculated from the corresponding neural activity. Mean membrane
687 potential was calculated from the subthreshold membrane potential occurring from 0 to 250 ms from
688 inhalation onset. Peak membrane potential was designated as the maximum membrane potential
689 within 30-250ms after inhalation onset, and time of the peak membrane potential was calculated at

690 the time of this maximum membrane potential relative to inhalation onset. Spike counts were
691 calculated by summing all action potentials occurring within the same timeframe. To calculate the
692 correlations for each parameter, each was averaged across all sniffs within the category and regression
693 analysis was used to generate an R and p value between the resulting average parameters and the
694 corresponding inhalation duration (minimum of the category). For each cell, inhalation duration
695 categories were excluded from the correlation if they contained less than 25 sniffs, and cells that had
696 less than 5 valid categories were additionally excluded. For shuffle controls, inhalation duration was
697 shuffled throughout the data and the regression analysis repeated 10 times per cell.

698 *Euclidean distance analysis of detectability of sniff change*

699 For this analysis only cells with more than 50 sniffs during baseline in each category: 55-65 ms, 75-85
700 ms and 95-105 ms inhalation duration were included. A random subset of 25 sniffs in each group were
701 selected and spike activity within these samples were used to construct PSTHs. PSTHs were put in
702 sequence, either 3 consecutive 95 ms inhalation duration sniffs (control sequence), or the same
703 sequence but with the final sniff of a different inhalation duration, either 75 ms or 55 ms. Each PSTH
704 was normalised such that the first 30 ms started at zero Hz on average. Euclidean distance across the
705 population of these sequences were then calculated between the control sequence and sequences
706 ending in 55 ms or 75 ms inhalation duration sniffs. Detection time for the change in inhalation
707 duration was calculated where the Euclidean distance in the last sniff exceeded the mean + 2 SDs of
708 the baseline Euclidean distance from the first 2 sniffs.

709 *Discriminability of slow and fast sniffs from emulated MC/TC population activity*

710 Sniff cycles from 42 recorded neurons (25 MC, 17 TC) were divided into fast (37-80 ms), medium (80-
711 96 ms) and slow (96-183 ms) cohorts. All cycles with sniff duration below the 0.5th percentile (108
712 ms) and above the 99.5th percentile (597 ms) were discarded. All cycles with inhalation duration
713 below the 0.5th percentile (37 ms) and above the 99.5th percentile (183 ms) were discarded. From
714 each cell the spiking activity for 400 ms (except for Figure 8D, where the length was varied) following

715 the inhalation onset in a randomly chosen fast or slow inhalation cycle was combined to create
716 emulated population spike trains (32 slow and 32 fast inhalation cycles). The emulated inhalation
717 cycles split to a training set (22 slow and 22 fast inhalation cycles) and a test set (10 slow and 10 fast
718 inhalation cycles). For each MC/TC neuron a postsynaptic EPSPs waveform (one sample per ms) was
719 simulated by convolving the spike train with a normalised alpha function (amplitude=10, time
720 constant: 10 ms, see Kollo et al. 2014). The compound EPSP of the read-out neuron was calculated as
721 the weighted linear sum of the individual EPSP waveforms of each cell (Figure S7). The read-out neuron
722 was activated if the maximum of the EPSP waveform crossed the threshold value. To find the optimal
723 values of EPSP weights and threshold, the Nelder-Mead method was used with a logistic activation
724 function in the read-out neuron. Discrimination performance of fast and slow inhalation cycles was
725 assessed on the test set with the Matthews correlation coefficient.

726 *Phase preference and putative MC and TC boundaries*

727 The theta modulation properties of each cell were calculated as previously (Fukunaga et al. 2012;
728 Jordan et al., 2017). Due to the high variability of sniff behaviour in awake mice, analysis was restricted
729 to sniff cycles between 0.25 and 0.3 s in duration, where the preceding sniff cycle was also within this
730 range. Mean V_m from the spike-subtracted V_m trace was taken as a function of sniff cycle phase for at
731 least 150 sniffs, and this was plotted as Cartesian coordinates. The angle of the mean vector calculated
732 by averaging these Cartesian coordinates was taken as the phase preference of the cell. To determine
733 putative MC or TC type based on phase preference, we used the phase boundaries calculated in a
734 submitted paper (Jordan et al. 2017).

735 *Modulation of sniff-activity relationships across phase preference*

736 In reference to Figure 7D and E. To determine whether the sign of relationships between inhalation
737 duration and the various activity parameters is modulated by the sniff phase preference of the cell, R
738 values for the various correlations were plotted as a function of phase preference. Only correlations
739 with a significant p value (<0.05) and with an R^2>0.6 were included. A sliding window of 2 radians was

740 then used to calculate the mean R value for all cells with phase preference within the window,
741 resulting in a mean R value as a function of phase preference. The modulation strength of mean R
742 value as a function of phase was then calculated: the plot of mean R value was normalised to the
743 minimum value across all phases, and the result plotted as Cartesian coordinates. The length of the
744 mean vector calculated by averaging these Cartesian coordinates was taken as the modulation
745 strength of the R value across phase space. To determine the significance of this modulation, R values
746 were shuffled with respect to phase preference 10000 times, and the resulting distribution of shuffled
747 modulation strength was compared to the value for the unshuffled data.

748 *Learning time and reaction time*

749 **Learning time:** For the generation of learning curves as in Figure 4, a moving window was used across
750 5 consecutive CS+ and 5 consecutive CS- trials, advanced by 1 trial on each step, and a percentage
751 correct calculated. The trial at which this reached 80% correct for 5 consecutive points was deemed
752 the learning time.

753 Reaction time calculations were based on 10 or more trials of 80% performance. **From lick behavior:**
754 For each CS+ and CS-, lick probability was calculated in a moving time window of 100 ms, aligned to
755 the first inhalation after final valve opening. The difference between the probability of licking for CS+
756 and CS- for each time window was calculated, and the leading edge of the first window at which this
757 calculated difference significantly deviated from the values calculated from the 2 s window prior to
758 odor onset was considered the reaction time. **From sniff behavior:** inhalation and exhalation duration
759 values were calculated for CS+ and CS- as a function of sniff number from odor onset. These values
760 were compared between those calculated for CS+ and CS- using a t-test, and the reaction time was
761 calculated based on the first inhalation or exhalation within the series to show a significant difference.

762 ## Supplementary Information

763 *Effect of sniff change and concentration change on sniff phase-aligned responses*

764 Given that using absolute latency, sniff parameters can render concentrations indiscriminable, it must
765 be the case that the coding of concentration takes sniff parameters into account. One way of doing
766 this would be to code relative to phase of the sniff cycle (Shusterman et al., 2011). We thus repeated
767 the above analysis, with spikes registered to phase of sniff cycle rather than absolute time.

768 First we looked at the effect of changing sniff speed on excitatory bursts across the 13 cell-odor pair
769 population as above (as done in Figure 2 for absolute time). When registered to phase, we noticed
770 that fast sniffing did not appear to evoke any consistent shift in excitatory response onset (Figure S4).
771 Overall there were variable changes in the detected onset phase between fast and slow sniffing, with
772 no significant systematic change seen (mean latency change = -0.17 ± 0.37 rad, n = 13, p = 0.12, paired
773 t-test; Figure S4B). The changes in phase-aligned responses due to sniff change look particularly small
774 and inconsistent when compared directly to those evoked by latency change (Figure S4C). The
775 difference was particularly obvious when comparing average change in mean spike count aligned to
776 the onset for slow sniffing: for latency aligned responses, there is a clear peak prior to onset that
777 corresponds to the advance of the excitatory bursts, while for phase aligned responses this is much
778 smaller (Latency: 0.47 ± 0.3 spk/bin, phase: 0.16 ± 0.18 spk/bin, p = 0.004, unpaired t-test, averaged
779 approx. 20 ms prior to onset; Figure S4D). Thus the ubiquitous advance of onset latency calculated
780 before is not present when registering to sniff cycle phase.

781 Using phases, increasing concentration again evoked an advance in excitatory bursts, however, unlike
782 for absolute latency, increasing the speed of the first sniff did not mimic this effect in the early
783 excitatory responses (Figure S4E). Directly comparing the phase changes evoked by increasing
784 concentration with those evoked by fast sniffing revealed that, in 3 of 4 cases, the change evoked by
785 concentration was larger. As for latency, the changes in the excitatory responses again contributed to
786 almost the entirety of the discriminability, as manually shifting the slow sniff responses forward

787 caused a dramatic reduction in discriminability (Figure S4G, ‘slow sniff adv.’). The remainder of the
788 discriminability seen was due to changes in the peak excitation, as excluding the four excitatory
789 responses altogether reduced discriminability to baseline (data not shown). However, unlike for
790 latency, faster sniffing did not cause a reduction in discriminability; if anything, it increased the
791 discriminability of the concentrations (Figure S4G, ‘fast sniff’).

792 Thus, taking sniff cycle phase into account enables concentration to be discriminated from the
793 olfactory bulb output regardless of changes in sniffing. This is congruent with the recent study that
794 compared several modes of time/phase-warping and time-shifting the spiking responses of cells in
795 how much they could improve concentration discrimination from the population spiking given high
796 variance in sniff dynamics (Shusterman et al., 2017). However, Shusterman and colleagues find that
797 phase-warping does not provide the best performance, and indeed we note that phase warped
798 responses still show very high variance as a function of sniff duration, particularly in peak response.

799

Supplementary Figures

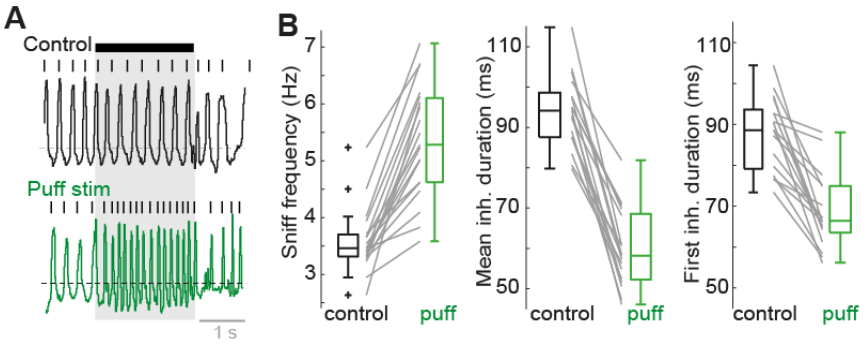

Figure S1. Effect of puff stimulus on sniff behaviour.

(**A**) Example nasal flow traces from one animal during a control trial (no puff stimulus accompanying 2 s odor stimulus) and a trial with a puff stimulus. Shaded area shows odor stimulus. (**B**) Plots to show average change in sniff frequency, mean inhalation duration, and first inhalation duration between five slow (black, control) and five fast (green, puff) trials for all 20 cell-odor pairs.

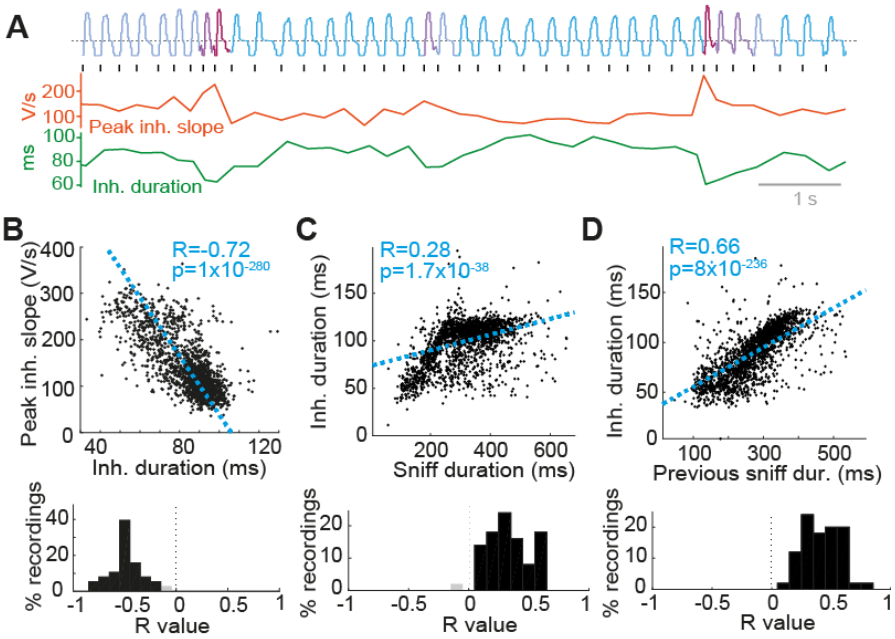

Figure S2. Correlations between different sniffing parameters.

(**A**) Example nasal flow trace during an inter-trial interval (no odor), with sniffs colored according to their inhalation duration (blue to red = long to short duration). Black ticks show time of inhalation onset, orange plot shows peak inhalation slope for each inhalation aligned to the inhalation onset, and green plot shows inhalation duration for each inhalation. (**B**) Example correlation between inhalation duration and peak inhalation slope for 1988 sniffs in 1 animal (top), and histogram of correlation R values between inhalation duration and peak inhalation slope across 50 animals. Black bars indicate significant correlations. (**C**) As for B, but for correlation between sniff duration and inhalation duration. (**D**) As for B, but for the correlation between the previous sniff duration and the current inhalation duration.

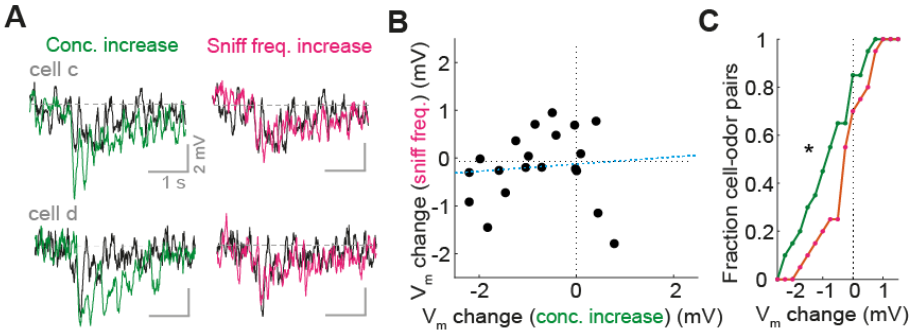

Figure S3. Changes in subthreshold response are more inhibitory for concentration increase than for fast sniffing.

(**A**) Example average subthreshold response traces for low concentration, slow sniffing (black), high concentration, slow sniffing (green) and low concentration, fast sniffing (magenta), for two different cells, cell c (top) and cell d (bottom). Each trace is the average of 5 spike-subtracted trials. (**B**) Scatter to show average change in membrane potential response for the first 1 s of the odor stimulus for concentration increase (high conc.-low conc.) and sniff frequency change (fast sniffing-slow sniffing). (**C**) Cumulative histograms of membrane potential response change for concentration increase (green) and sniff frequency increase (magenta). P = 0.03, paired t-test.

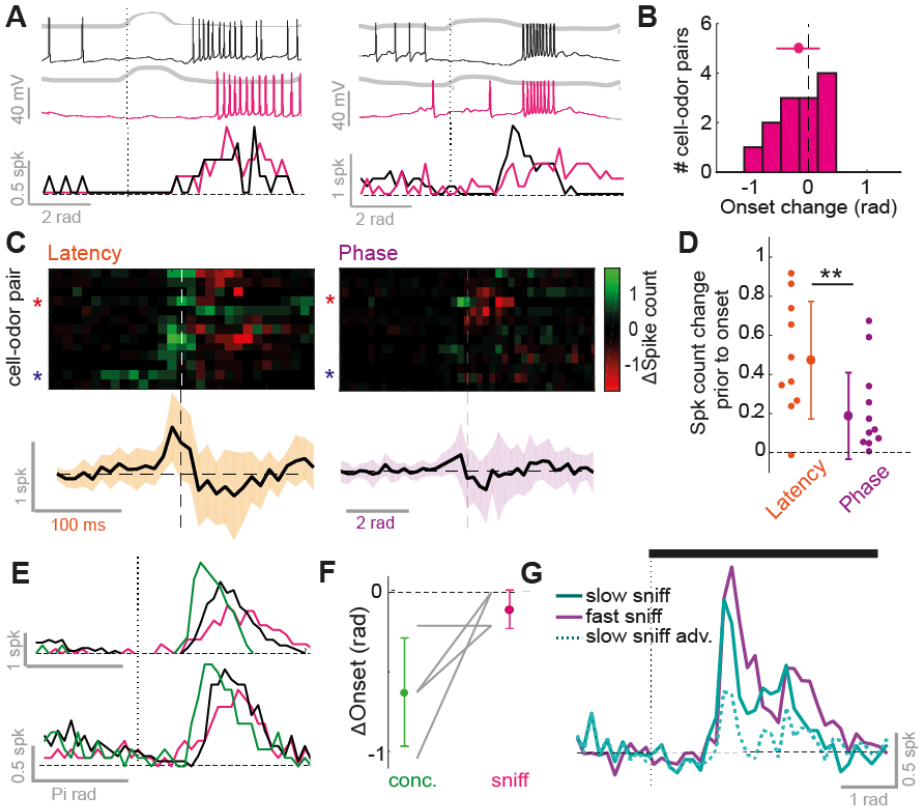

Figure S4. Fast sniffing does not replicate effect of concentration change when aligning to sniff phase.

(**A**) Example trace, and corresponding mean spike counts for early excitatory responses for both slow inhalation (black) and fast inhalation (pink), for two different cell-odor pairs, with each time-point warped to the phase of the sniff cycle. (**B**) Histogram of phase onset changes (fast-slow) for all 13 cell-odor pairs. (**C**) Above: heatmaps of the change in mean spike count between fast and slow sniffs for all 13-cell-odor pairs, aligned to their response onset at slow sniffing (dashed vertical line). On the left shows the data in absolute time after inhalation onset, while the right heatmap shows the same data warped to sniff phase. Below: plot shows mean change in spike count across the above sample of 13 cell-odor pairs. Shaded area shows standard deviation. (**D**) Mean change in spike count between fast and slow sniffs in the 20 ms time window prior to response onset at slow sniffing for all 13 cell-odor pairs, compared where responses were aligned to absolute time, or sniff phase. (**E**) Example mean spike counts for two early excitatory responses registered to the phase of the sniff cycle. Black shows response at low concentration for slow inhalation, pink shows response at low concentration for fast inhalation, and green shows response for high concentration and slow inhalation. (**F**) For the 4 early excitatory cell-odor pairs in the dataset (as in Figure 3), a comparison of the change in response onset phase when concentration is changed from low to high (green data), and when the sniff was changed from fast to slow (magenta data). *Continued on next page…*

(**G**) Euclidean distance over time between population vectors for high and low concentration spike counts where the inhalation was slow ('slow sniff'; solid cyan), for high concentration and time-shifted low concentration where excitatory phase changes due to concentration change were undone via time shifting of the data ('slow sniff adv.'; dotted cyan), and for high concentration and low concentration where low concentration data came from fast inhalation trials ('fast sniff'; solid purple). Spike counts for population response vectors were registered to sniff phase.

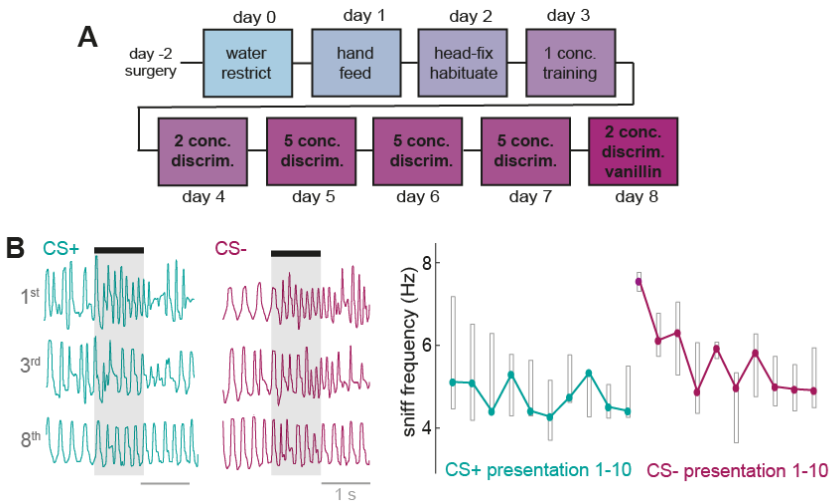

Figure S5. Additional behavioral data.

(**A**) Diagram to show training sequence for mice (described in methods). (**B**) Left: Example sniff traces for the 1st, 3rd and 8th presentation of the CS+ and CS- concentrations for the initial concentration discrimination session. Note that in this session, the CS+ concentration is first presented 10 times to ensure retention of the lick pattern learned the day before, and then the CS- is interleaved in a pseudorandom order. Right: plot to show median sniff frequency across 8 mice (regardless of concentration contingency) for presentations 1-10 of the CS+ and CS- concentration in the first 2 concentration discrimination session. Boxes show upper and lower quartiles.

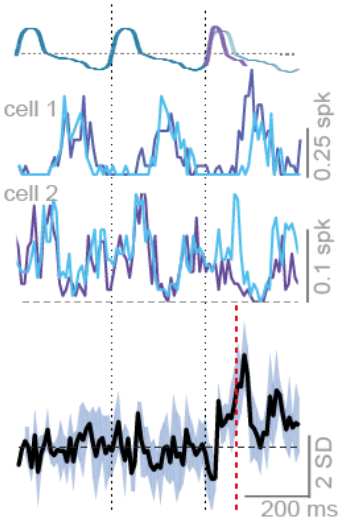

Figure S6. Detection of inhalation duration change between 55 and 75ms.

As for Figure 8A & B, this time comparing PSTHs for a smaller inhalation duration change (95 ms, blue to 75 ms, purple).

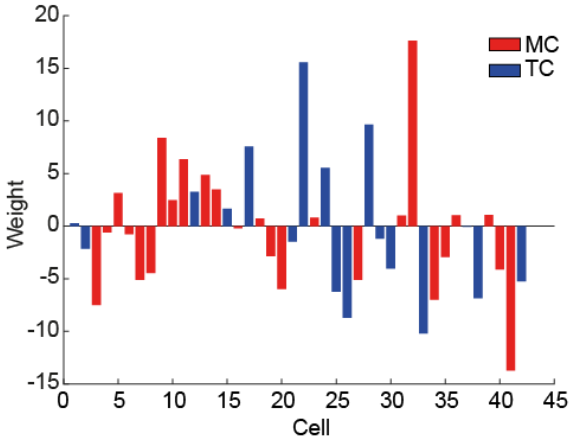

Figure S7. MTC synaptic weights in simulated network for inhalation duration discrimination.

In reference to Figure 8C-D. Synaptic weights for individual MTCs in an emulated population after training of a simple neural network to distinguish fast and slow inhalations (see methods).

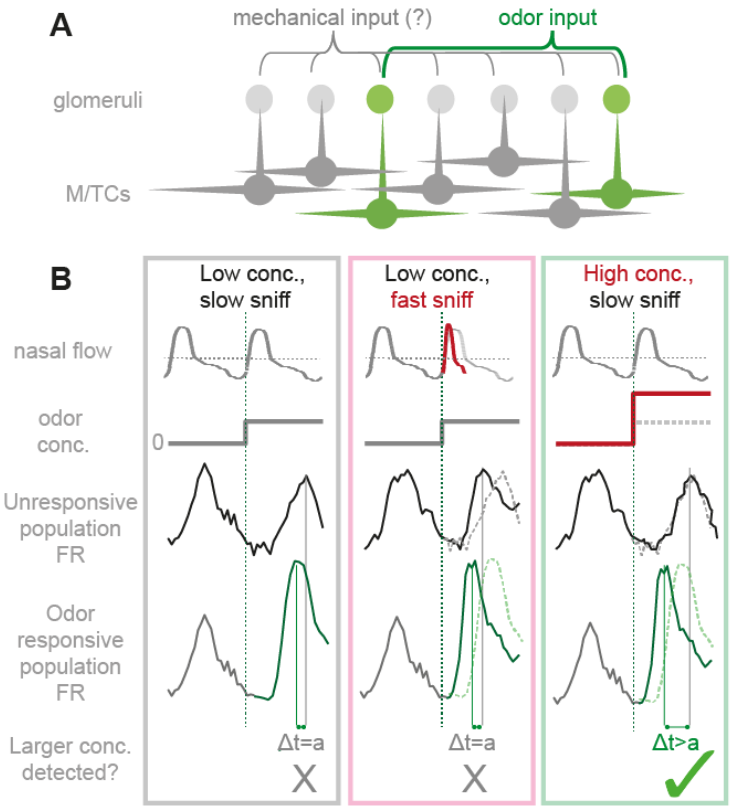

Figure S8. Diagram of a potential relative timing code for concentration.

(**A**) Highly simplified diagram of the olfactory bulb, depicting only glomeruli and MTCs. Green glomeruli/MTCs show those receiving odor input (odor responsive), while grey glomeruli/MTCs show those with absence of such input (unresponsive population). While odor inputs are sparse, mechanical input (response to the pressure change associated with each sniff) is widespread. (**B**) Diagram to show how a relative time code may work. Each instance shows one sniff prior to and during odor stimulation. 'Nasal flow' shows these two sniffs, with grey showing slow sniffs (>95 ms inhalation duration) and red showing a fast sniff (e.g. 55 ms inhalation duration). 'Odor concentration' trace shows a step increase in concentration from zero just prior to the second sniff. Grey traces show low concentration and red shows high concentration (2 x low concentration). 'Unresponsive population' shows a hypothetical population average FR for all cells without odor inputs during the odor stimulus. Dotted traces in second and third column for the second sniff cycle show the trace for the first column, for sake of comparison. 'Odor responsive' shows the average population FR for cells receiving direct odor input. Dotted traces in second and third column for the second sniff cycle show the trace for the first column, for sake of comparison. Δt shows the difference in peak population activity for unresponsive and odor-responsive cells during the stimulus. Note that Δt remains stable unless the concentration changes, and not when the sniff alone changes. A change in Δt allows perception of a different concentration.